Sam Haarto

A 22 GHz prototype receiver for continuous comparison polarimetry

School of Electrical Engineering

Thesis submitted for examination for the degree of Master of Science in Technology.

Espoo March 9, 2016

Thesis supervisor:

Prof. Anne Lähteenmäki

Thesis advisors:

D.Sc. (Tech.) Kaj Wiik

M.Sc. (Tech.) Petri Kirves

Aalto-yliopisto
School of Electrical Engineering

AALTO UNIVERSITY
SCHOOL OF ELECTRICAL ENGINEERING

ABSTRACT OF THE
MASTER'S THESIS

Author: Sam Haarto

Title: A 22 GHz prototype receiver for continuous comparison polarimetry

Date: March 9, 2016 Language: English Number of pages: 7+51

Metsähovi Radio Observatory & Department of Radio Science and Engineering

Professorship: Space Technology and Science Code: ETA3001

Supervisor: Prof. Anne Lähteenmäki

Advisors: D.Sc. (Tech.) Kaj Wiik, M.Sc. (Tech.) Petri Kirves

Radio astronomy is a subfield of astronomy that studies celestial objects that emit radio waves. As radio waves can penetrate dust, radio astronomy can study things that can't be seen in visible light. Radio astronomy studies the Sun, planets, gas and dust clouds of the Milky Way, pulsars, radio galaxies, quasars and cosmic background radiation.

Polarimetry has been a quite recent addition to radio astronomy. Polarimetry studies the polarization of light and other transverse waves. The applications are present in a variety fields of astrophysics ranging from solar physics to cosmology. Polarimetry can be used to study for example the strength and orientation of magnetic fields in the space between planets in the Solar system and other planetary systems. It has given us insight into physical processes occurring in systems that range from our own solar system to high-redshift galaxies.

The goal of this thesis was to build a prototype receiver for continuous comparison polarimetry. This prototype would be used as a testing device for the back-end planned for the Metsähovi's continuous comparison receiver. With this prototype receiver, one hopes to find and solve the possible problems that the final receiver might have, and also to ease with the adaptation of the new back-end. In addition to building a prototype receiver, the importance of polarization in radio astronomy was presented.

Although a working prototype could not be achieved during this thesis an insight into the designing process was given. Designing, manufacturing and debugging of different components of the receiver was shown and future plans for the prototype was presented. Quite lossy 180° hybrids were produced. To proceed with the back-end testing new amplifier cards and a working back-end module should be acquired. Furthermore, the orthomode transducers of the prototype also need further testing to ensure their validity.

Keywords: Radio astronomy, receiver, continuous comparison, polarimetry.

AALTO-YLIOPISTO
SÄHKÖTEKNIIKAN KORKEAKOULU

DIPLOMITYÖN
TIIVISTELMÄ

Tekijä: Sam Haarto

Työn nimi: 22 GHz vastaanottimen prototyyppi jatkuva-vertailu polarimetriaan

Päivämäärä: March 9, 2016 Kieli: Englanti Sivumäärä: 7+51

Metsähovin radiotutkimusasema & Radiotieteen ja -tekniikan laitos

Professuuri: Avaruustekniikka ja -tiede Koodi: ETA3001

Valvoja: Prof. Anne Lähteenmäki

Ohjaajat: TkT Kaj Wiik, DI Petri Kirves

Radioastronomia on astronomian osa-alue, joka tutkii radioaaltoja lähettäviä taivaankappaleita. Koska radioaallot läpäisevät pölyn, radioastronomia pystyy tutkimaan asioita, joita ei näe silmin. Radioastronomia tutkii Aurinkoa, planeettoja, Linnunradan kaasu- ja pölypilviä, pulsareita, radiogalakseja, kvasaareja ja kosmista taustasäteilyä.
Polarimetria on melko uusi lisäys radioastronomiaan. Polarimetria tutkii polarisoitunutta valoa ja muita aaltomuotoja. Sen sovelluskohteita löytyy useilta eri astrofysiikan alueilta, aurinkotutkimuksesta aina kosmologiaan. Polarimetrian avulla pystytään tutkimaan esimerkiksi Aurinkokunnan ja muiden planeettakuntien magneettikenttien voimakkuuksia ja niiden suuntia. Nämä tutkimukset ovat valaisseet tietämystämme eri fyysisistä prosesseista, joita tapahtuu Aurinkokunnassamme kuin myös kaukaisissa galakseissa.
Tämän diplomityön tavoitteena on valmistaa vastaanottimen prototyyppi jatkuva-vertailu polariametriaan. Tätä prototyyppiä olisi tarkoitus käyttää Metsähovin uuden jatkuva-vertailu vastaanottimen taustajärjestelmän testaamiseen. Tavoitteena on löytää ja ratkaista mahdolliset ongelmat, joita uudessa vastaanottimessa havaitaan. Lisäksi prototyyppi helpottaa uuden taustajärjestelmän käyttöönotossa. Diplomityö esittelee myös kuinka tärkeäksi osaksi polarisaatio on noussut radioastronomiassa.
Vaikka toimivaa vastaanottimen prototyyppiä ei tämän diplomityön aikana onnistuttu valmistamaan, itse suunnittelutyön prosessia havainnollistettiin onnistuneesti. Prototyypin eri osien suunnittelu, valmistus ja testaus esiteltiin sekä projektin tulevaisuuden näkymät kerrottiin. Melko häviöllinen 180° hybridi valmistettiin. Jotta taustajärjestelmää päästäisiin koestamaan, tulisi ensin hankkia toimivat vahvistinkorttit sekä uusi vastaanottimen takapää. Lisäksi prototyypin polarisaation haaroitin vaatii tarkempia kokeita sen toimivuuden varmistamiseksi.

Avainsanat: Radioastronomia, vastaanotin, jatkuva-vertailu, polarimetria.

Preface

First, I would like to thank my instructor Petri Kirves for helping me with the thesis and with the manufacturing of the different components of the prototype. Also, a thanks to my other instructor Kaj Wiik for helping me with the theoretical side of continuous comparison receivers and introducing me to polarimetry.

I would also like thank my supervisor and professor Anne Lähteenmäki for introducing me to the thesis topic and for introducing me to Metsähovi radio observatory as a work place. A special thanks to everyone at Metsähovi for providing a warm and welcoming environment and helping with my thesis. Also a thanks to those RAD employees that helped me with different testing equipment and simulation softwares.

Kudos to my friends for all the help and advice that I have received during my studies. Finally, I would like to express my gratitude to my loving wife and family and thank them for supporting me.

Otaniemi, March 9, 2016

Contents

Symbols and abbreviations

Symbols

B_n	Noise bandwidth
p	Degree of polarization
p_{circ}	Degree of circular polarization
p_{lin}	Degree of linear polarization
ΔT	Minimum detectable noise difference
T_A	Antenna noise temperature
T_R	Receiver noise temperature
τ	Integration time of the detector output voltage

Abbreviations

AGN	Active Galactic Nuclei
CMB	Cosmic microwave background
COTS	Commercial off-the-shelf
DSB	Double sideband mixer
IF	intermediate frequency
LNA	Low noise amplifiers
LO	Local oscillator
MRO	Metsähovi Radio Observatory
NIR	Near-infrared
OMT	Orthomode transducer
PLL	Phase lock loop
PTFE	Polytetrafluoroethylene
RMS	Root mean square
SMD	Surface-mount device
SMA	SubMiniature version A
UHF	Ultra high frequency
VCO	Voltage controlled oscillator
VHF	Very high frequency
VLBI	Very-long-baseline interferometry
YIG	Yttrium-Iron-Garnet

Materials

$(C_2F_4)_n$	Polytetrafluoroethylene
C_3H_6O	Acetone
$FeCl_3$	Ferric chloride
NaOH	Sodium hydroxide

1 Introduction

Radio astronomy is a subfield of astronomy that studies celestial objects that emit radio waves. Measurements on the surface are limited by the so-called radio window that restricts the range of frequencies of electromagnetic radiation that can pass through Earth's atmosphere. The atmosphere is nearly transparent at zenith from about 10 MHz to tens of GHz, where the reflections from ionosphere sets the lower frequency limit. At millimeter and submillimeter wavelengths, the water vapour in the atmosphere can attenuate the signals severely, hence radio telescopes must be placed in relatively drier site, like on mountain tops or even satellites. As radio waves can penetrate dust, radio astronomy can study objects that can't be seen in visible light. The mechanisms driving the radio and optical radiation are different from each other. Therefore, radio astronomy has revealed many new objects and phenomena that could not be observed in the optical, for example the cosmic microwave background (CMB) radiation was first detected using radio telescopes [1]. Observations in the radio are used for the studies of the Sun, planets, gas and dust clouds of the Milky Way, pulsars, radio galaxies, quasars and cosmic background radiation. In addition to this, they are also used for researching extraterrestrial intelligence.[2, 3]

Through polarimetry one studies the polarization of light and other transverse waves. It can be used to study for example the strength and orientation of magnetic fields in the space between planets in the Solar system and other planetary systems.[3]

The light of most stars is unpolarized, which is why they are used as reference sources for optical zero-polarization instead of lamps. The reason for this low polarization is the great distance and the spherical symmetry of most stars. These circumstances are the main reason why polarimetry is such a late addition to astronomy. Polarimetry remained a specialist technique even in the most advanced instruments; with solar physics being the notable exception [4]. Due to the lack of attention to polarimetry, awareness of polarization-induced photometric errors within telescopes and instruments has been minimal.

However, during the last few decades, considerable progress has been made by polarization specialist. Astronomers now realize not to neglect polarization and know that whenever there is substantial asymmetry in an astronomical situation, there might be polarization at some level. The higher the resolution, the larger, in general, is the polarization.[4]

Polarimetry has application in a variety fields of astrophysics ranging from solar physics to cosmology. It can provide information about the physics of the targets that cannot be obtained in any other way. This is probably the main reason behind the decision to build a new continuous comparison receiver for the 14-meter radio telescope in Metsähovi Radio Observatory (MRO).

The goal of this thesis is to build a prototype receiver for continuous comparison polarimetry. This prototype is to be used as a testing device for the back-end planned for the Metsähovi's continuous comparison receiver. With this prototype receiver, one hopes to find and solve the possible problems the final receiver might

have and to ease with the adaptation of the new back-end. This thesis will also present the process of designing and testing a prototype receiver. The goal is to show the reader what it is like to design a prototype, what was done right, what can be improved, and what should have been done differently. Secondary goals of the thesis are to inform the reader about the importance of polarization and why polarimetry has become a so important tool in radio astronomy.

After this chapter the structure of the thesis is as follows: Chapter 2 gives a glance at the history of radio astronomy and introduces the main equipment used in MRO. Chapter 3 explains polarization and describes its different forms. Chapter 4 introduces the Stokes parameter which will help in describing polarization. Chapter 5 focuses on polarimetry and explains why it is so important tool in astronomy. Chapter 6 introduces different types of radio astronomy receivers. Chapter 7 focuses on the various components of the prototype receiver. Chapter 8 describes the design and manufacturing process of a 180° hybrid used in the prototype receiver. Chapter 9 focuses on the assembly, and testing of the Orthomode transducer(OMT) used in the prototype. Chapter 10 recounts the design, assembly and testing of the amplifier card. Chapter 11 concludes the thesis with a brief summary and a glance to future plans for the receiver and the prototype.

2 Background info

2.1 Brief history of radio astronomy

Radio astronomy was born in the 1930s. The first radio observations of the stars were made accidentally. In the years 1931 and 1932 the American engineer Karl Jansky was studying interference in communications produced by thunderstorms. In addition to the known interferences produced by thunderstorm he observed a weak and steady signal. At first it seemed that this signal was coming from the Sun but after continuing these observation he found that the source of the interference was moving away from the Sun. After more than a year of observation in December, 1932, Jansky deduced that noise was coming from the Milky Way.[5]

At first Jansky's findings didn't attract the attention of astronomers as back then they were not aware of celestial objects that produced radio signals. However, the American radio engineer Grote Reber was intrigued by this discovery as amateur astronomer. He built a fully steerable parabolic reflector and observed tens of radio sources in the sky. His first receiver for radio astronomy was built in 1938 and later in 1941 he finished the first radio map of the sky [5]. The Second World War accelerated the developments of radio technology with the high demand for wireless communication and radars. After World War II, improved receivers allowed the radio window to develop.

In the early days the studies concentrated on relatively long wavelengths, because the antennas and receivers were easier to build for longer wavelengths. Later on, a much studied wavelength was 21 cm or 1420 MHz, which is used to study the interstellar neutral hydrogen. The spectral line of hydrogen was first observed in 1953. In the 1960s microwave technology became available to astronomers as antennas and receivers developed further. The historical development has been towards higher sensitivity, shorter wavelength, and higher angular resolution [6].[2, 3]

2.2 Main telescope at Metsähovi Radio Observatory

Parabolic bowl are used as an antenna in radio telescopes. It reflects the radiation back towards the receiver in primary focus. Usually, however, telescopes have a secondary convex mirror which redirects the radiation towards a hole at the center of the main mirror, where the receiver lies. This setup is called a Cassegrain telescope and is used often in radio antennas and optical telescopes.

The main telescope used in Metsähovi Radio Observatory is a Cassegrain reflector mounted on a altitude-azimuth mount. It has a primary reflector with a diameter of 13.7 m. The reflector structure was updated in 1992 to a new one with a 0.1 mm surface accuracy. This with the protective dome, that was updated in 1994, allow observing frequencies up to about 250 GHz, although it has only been tested at 150 GHz. The dome protect the antenna from weather elements but lets radio frequencies through.

The main telescope was built in 1973 and the first observations were done in 1974. Since then, the telescope has been used actively in observing extragalactic

radio sources, the Sun and in astronomical and geodetic Very-long-baseline interferometry (VLBI) observations. The most used frequencies are 37 GHz and 22 GHz for continuum observations of quasars and of the Sun. Astronomical VLBI is conducted in 22, 43 and 86 GHz whereas the geodetic VLBI uses a dual band 2 / 8 GHz receiver.[7]

3 Description of polarized radiation

Electromagnetic radiation consist of transverse vibration of the electromagnetic field. When signals exhibit lasting phase and amplitude relations between them, the wave is said to be polarized. In astronomy, generally only a part of the radiation is polarized and the rest remain unpolarized. The polarized part can be a function of direction of arrival, time or wavelength. Depending on the extent of this organized pattern, the wave is said to be fully polarized, partially polarized or unpolarized. The shape of the pattern can also be specified as linear, circular or elliptical. This dependency can be expressed as a degree of polarization, in which most of the astronomical information from polarimetry resides.[4]

This chapter will describe what polarized radiation is, starting from the most specific form of polarized radiation and then move gradually towards the most generic form. Polarized radiations are divided into linear, circular and elliptical radiation.

3.1 Linear polarization

A monochromatic linearly polarized wave has a transverse electric field with constant orientation. It has a constant amplitude and frequency varying strictly sinusoidally with time. The duration of this wave is infinite. Closest real life example of this is a monochromatic laser that is passed through a Polaroid.

A monochromatic wave becomes quasi-monochromatic if its amplitude and phase is allowed to vary slowly and often even randomly. The faster these so-called slow variations are, the broader the range of frequencies contained in within the wave. It will still be fully polarized as long as it isn't modified any further. A good approximation for quasi-monochromatic radiation is the light from a filament lamp that is filtered with a monochromator and a Polaroid.

Fully linearly polarized polychromatic radiation is a superposition of quasi-monochromatic waves of many different frequencies. There is usually no stable phase relation between the electromagnetic field at different frequencies, and no single dominant frequency, phase or amplitude exist. Only the unique orientation of the field ties them together. There exist no clear line between quasi-chromatic and polychromatic radiation. In practice, the fractional bandwidth is the criterion.[4]

3.2 Circular polarization

A monochromatic circularly polarized wave is a combination of two orthogonal monochromatic linearly polarized waves with equal amplitude and a phase difference of $\pm 90°$. The combined electric field vector has a constant magnitude and revolves uniformly per wave period, either left or right according to the sign of the phase difference. Being monochromatic, the wave has infinite duration.

As in linearly polarized waves, the quasi-monochromatic fully circularly polarized wave differs from monochromatic only by slow and often random variations of the amplitude and rotating velocity. The wave frequency is on average the same but the electric field vector moves around the mean position on the circle, also the circle

changes slowly. For usual astronomical signals, the slow drifts in circle size and in position on the circle are both random.

Polychromatic circularly polarized radiation is a superposition of quasi-monochromatic waves of many different frequencies, but all circularly polarized in the same way. As in the linearly polarized equivalent, there is no stable phase relation between waves at different frequencies.[4]

3.3 Elliptical polarization

Elliptical polarization is the most general form of polarization and linear and circular polarization are special cases of this. The defining parameters of an ellipse are axis ratio, handedness and orientation. Linear polarization has an axis ratio of 0 and circular polarization an axis ratio of 1.

A monochromatic elliptically polarized wave can be seen as a sum of two unequal linearly polarized components with a phase difference of $\pm 90°$, or as the sum of two linearly polarized components with a phase difference of something else than $0°$or $\pm 90°$.

Quasi-monochromatic 100% elliptically polarized wave differs from the aforementioned monochromatic one by allowing the size of the ellipse to vary slowly. As was with the circularly polarized radiation, polychromatic 100% elliptically polarized radiation is a sum of quasi-monochromatic components, all with the same elliptical polarization.[4]

4 Stokes parameters

The Stokes parameters are a convenient way to describe the polarization state of electromagnetic radiation. The Stokes parameters are often displayed in a 4-vector S with components labelled I, Q, U, and V. These parameters describe either a single wave or a sum of many waves. If the electric field vector $\mathbf{E}$ is expressed in terms of x- and y-components as:

$$\mathbf{E} = (\hat{\mathbf{x}} E_x e^{i\Phi_1} + \hat{\mathbf{y}} E_x e^{i\Phi_2}) e^{i\omega \mathbf{t}}. \tag{1}$$

The Stokes vector can be written in terms of amplitudes E_x and E_y, and their relative phase $\delta = \Phi_1 - \Phi_2$ as:

$$S = \begin{pmatrix} I \\ Q \\ U \\ V \end{pmatrix} = \begin{pmatrix} E_x^2 + E_y^2 \\ E_x^2 - E_y^2 \\ 2E_x E_y \cos\delta \\ 2E_x E_y \sin\delta \end{pmatrix}. \tag{2}$$

The I represents the total power, Q the difference of vertical and horizontal power components, and U describes the plane of the polarization and V represent the ellipticity of the fully polarized wave.[8, 9]

Cosmic radio sources emit broad-band, partially polarized radiation. In the fully monochromatic wave the amplitudes and relative phase of two orthogonal components are constant but in a grouping of incoherent sources, e.g. a source of radio noise, the amplitudes and relative phase varies in time. Therefore a generalized time-averaged Stokes parameters are usually used in radio astronomy. For a broad-band source of radiation the time-averaged Stokes parameters are as follows:

$$S = \begin{pmatrix} I \\ Q \\ U \\ V \end{pmatrix} = \begin{pmatrix} < E_x^2 > + < E_y^2 > \\ < E_x^2 > - < E_y^2 > \\ < 2E_x E_y \cos\delta > \\ < 2E_x E_y \sin\delta > \end{pmatrix}. \tag{3}$$

These equations apply for a linear input. For circular input the Stokes parameters are:

$$S = \begin{pmatrix} I \\ Q \\ U \\ V \end{pmatrix} = \begin{pmatrix} < E_r^2 > + < E_l^2 > \\ < 2E_r E_l \sin\delta > \\ < 2E_r E_l \cos\delta > \\ < E_r^2 > - < E_l^2 > \end{pmatrix}. \tag{4}$$

The E_x is replaced with the right circularly polarized amplitude, E_r, the E_y is replaced with the left circularly polarised amplitude, E_l, and finally the Stokes Q and V are swapped.[9]

This is not the only definition for the Stokes parameters and the more commonly used in astronomical polarimetry are defined in term of the polarization ellipse, seen in Figure 1. Stokes parameters can be defined using polarization ellipse parameters

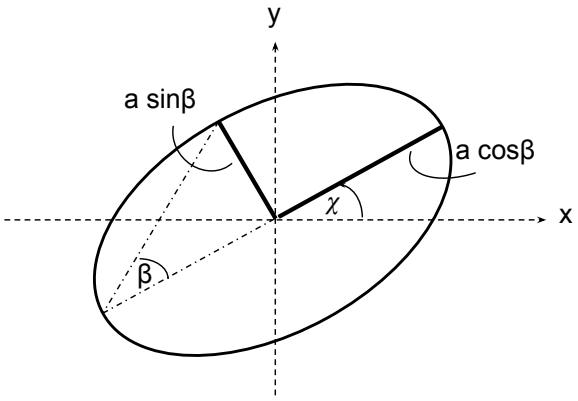

Figure 1: polarization ellipse.

as follows:

$$S = \begin{pmatrix} I \\ Q \\ U \\ V \end{pmatrix} = \begin{pmatrix} a^2 \\ a^2 \cos 2\beta \cos 2\chi \\ a^2 \cos 2\beta \sin 2\chi \\ a^2 \sin 2\beta \end{pmatrix} \tag{5}$$

where a is a quantity related to the amplitude of the electric field vibration, χ is the polarization angle and $\tan\beta$ is the axial ratio of ellipse. It can be seen that the intensity I must be zero or larger, where as Q, U, V can be either positive or negative.[4]

These Stokes parameters translate to polarization. For 100% polarization $Q^2 + U^2 + V^2 = I^2$. In general, 100% elliptical polarization is represented by non-zero vales of Q, U and V. For circular polarization $\sin\beta = \pm\cos\beta$ or $\sin(2\beta) = \pm 1$, $Q = U = 0$ and $|V| = a^2 = I$. For linear polarization either $\sin\beta$ or $\cos\beta$ is zero, which means that $\sin(2\beta) = 0$ and therefore $V = 0$, whereas $Q = a^2\cos(2\chi)$ and $U = a^2\sin(2\chi)$.

In unpolarized radiation no single polarization form dominates or is conspicuously absent. This can be achieved when two equal quasi-monochromatic or polychromatic 100% polarized waves of orthogonal polarization forms are combined. The aforementioned slow variation of amplitude and phase will be there at the beginning but after sufficiently long time interval, all possible forms of polarization will occur and the time-averaged Stokes parameters will be $< a^2 >, 0, 0, 0$, where $<>$ denotes time averages. It does not matter what polarization form is chosen, as long as the sum of the waves results in the Stokes vector: $I, 0, 0, 0$, i.e. the last three Stokes parameters are equal but opposite in the two components.

Partially polarized radiation is the incoherent sum of an unpolarized and a fully polarized component. Because the Stokes parameters of the partially polarized radiation are the sums of the Stokes parameters of the components, $Q^2 + U^2 + V^2 <$

I^2. The degree of polarization

$$p = \frac{\sqrt{(Q^2 + U^2 + V^2)}}{I} \tag{6}$$

is often used in astronomical polarimetry. Also the degree of circular polarization

$$p_{circ} = \frac{V}{I} \tag{7}$$

and the degree of linear polarization

$$p_{lin} = \frac{\sqrt{(Q^2 + U^2)}}{I} \tag{8}$$

are often encountered in literature.[4]

It doesn't matter which two orthogonal 100% polarizations one measures and adds together, be it orthogonal circular, two orthogonal linear at any pair of angles, or even orthogonal elliptical, they always give the total intensity I [10].

To combine polarizations, one must use the Stokes parameters. Fractional polarization will always be positive and will therefore never average to zero. The fractional polarizations must be converted into Stokes parameters, average the Stokes parameters, and then finally convert the Stokes parameters back into fractional polarization and position angle.

Unlike optical astronomers, radio astronomers can measure all the Stokes parameters simultaneously. This is done by subtracting, adding or multiplying electric fields of two orthogonal polarizations belonging to a different Stokes parameter.[10]

5 Polarimetry in astronomy

Polarimetry has application in various fields of astrophysics ranging from solar physics to cosmology. Polarimetry has given us insight into physical processes occurring in systems that range from our own solar system to high-redshift galaxies. Polarimetry was even used to study the nature of planetary surfaces and atmospheres as one of its earliest application.[11] It can provide information about the physics of the targets that cannot be obtained in any other way.

5.1 Birefringence

Two polarizations are said to be orthogonal to each other when the pair has the same I but the opposite Q, U and V. These waves will have the same axial ratio of ellipse but the axis are at a right angle and the ellipses will trace out in the opposite direction. Such pairs are independent solutions of Maxwell's equation, and they can propagate independently through empty space and other homogeneous isotropic media.

In homogeneous isotropic medium, all polarization modes have the same propagation velocity. However, in astronomical plasma, which can be found in e.g. solar active region, the Earth's ionosphere and interstellar medium, different polarization modes have different propagation velocities. These medium have always two orthogonal modes, called eigenmodes that can propagate through the medium without changing their polarization form. These eigenmodes depend on a given plasma and a given direction of the propagation with respect to the magnetic field. Because the polarization form is unchanged, it means that the modes are travelling at a different velocities. Which means that the medium has two refractive indices, one for each eigenmode. This kind of medium is said to be birefringent.

In general birefringence will be elliptical, i.e. the eigenmodes are elliptical. In linear birefringence, the eigenmodes are linear. For every other polarization angle, including circular polarization, the polarization form will change as the radiation passes through the medium. Circular birefringence causes relative phase shifts between two circularly polarized eigenmodes. A linearly polarized signal's direction of vibration will be rotated by the medium. In ionized plasma with a magnetic field component along the line of sight, such a rotation is called Faraday rotation. In radio astronomy, Faraday rotation is used to investigate the interstellar magnetic fields [6].[4]

5.2 Importance of polarization

Polarization can provide information about the strengths and orientation of magnetic fields, the distribution and orientation of scattering particles like dust grain, the microscopic structures of reflecting surfaces, or intrinsic anisotropies of the primordial plasma filling the early universe.[12] Polarization yields information about asymmetry or anisotropy inherent in astronomical configuration. This asymmetry can lie within the source, in the medium between the observer and the source, or both. The wavelengths used in polarimetry varies from γ-rays to meter radio waves. Using range of wavelengths it is possible to observe asymmetries in different parts of the same object.

The main asymmetries giving rise to astronomical polarization are magnetic fields and an asymmetric distribution of scattered radiation. Magnetic fields in astronomy range from 10 μG in interstellar space to perhaps 10^{13} G in pulsars.[4]

Polarimetry can also be used to find and confirm magnetic white dwarfs. Multiband time-resolved polarimetry is essential to the study of the internal structures of close binaries with magnetic white dwarf component. Information about the magnetic field configuration and radiation mechanism of pulsars can be found by measuring the polarization variations during its radio pulses. Historically, polarimetric observation of Crab nebula, the supernova remnant surrounding the Crab pulsar, provided the first ever evidence for synchrotron radiation from astronomical objects [12].

Polarimetry in radio domain has been used to study many other supernova remnants to obtain the magnetic field configuration.[4] A single measurement of linear polarization of a nonthermal source yields direct information about the mean direction and level of ordering of the magnetic field. One can potentially determine the geometry of the magnetic field in blazars by combining millimeter wave VLBI imaging in both total and polarized intensity with constant monitoring of the polarization in blazars. The high angular resolution of VLBI can be applied to a lower angular resolution data, e.g. optical measurements, if an identical fluctuation of the polarization angle is observed in both blazar measurements. This identical fluctuation of the polarization angle informs us that the electromagnetic radiation originates from the same place in both measurements. The geometry of the magnetic field is the key element to solve the physical processes in the relativistic jet,which are jets of matter with speeds close to the speed of light.[13, 14]

5.3 Sources of polarization

All sources of radiation, at some level, are polarized, and it is likely that a completely unpolarized source is unachievable. The polarization is produces in a variety of ways, including directly from radiation processes, from different absorption of radiation passing through the interstellar medium, and also from scattering of radiation. Fractional polarizations of interest to astronomers range from tenths to parts per million.

The measured polarization of the Sun is low, and almost every other object in the

sky has a higher polarization. Our neighboring planets, seen in reflected light from the Sun at visible and near-infrared (NIR) wavelengths, have polarizations reaching up to several tens of per cent, dependent on the angle between the Sun, the measured planet and the Earth. If the Sun were much further away from the Earth a higher polarization would be measured, and it would increase with distance.[11]

The interstellar polarization of scattered starlight is due to the interplay of interstellar dust and galactic magnetic fields. The linear polarization of interstellar polarization ranges from few to about ten per cent.[12] The interstellar polarization is produces by dielectric dust grains, typically of size 0.1 μm. The dust is spread around the interstellar space and attenuate and redden the radiation[11]. They also produce some polarization by absorption, and therefore must be non-spherical.

High spin rates for such grains, which aid grain alignment, is produced by radiative torques. This was first proposed in the early 1970, but was forgotten for several decades. Now this mechanism is thought to be an important process. Key feature of the grain alignment is that the short axis of the gain invariably aligns with the local magnetic field, unlike compass needles. This is due to the rapid precession of the grains about the magnetic field, arising from the magnetic moment induced in the paramagnetic dust grain. Radiation with the electric field vector parallel to the long axis of the grain is preferentially absorbed, leading to a net polarization parallel to the grain short axis, and therefore along the direction of the magnetic field. This process is also known as dichroic absorption. This differential extinction of starlight has been used to map the magnetic field in our own galaxy. At millimeter and submillimeter wavelengths the aligned dust grains produce polarization in emission, rather than absorption, with the electric vector now perpendicular to the local magnetic field.

Magnetic fields in the dusty molecular clouds are believed to be in an important role in the most phases of star formation, including the initial collapse of the cloud and the ubiquitous outflows. These magnetic field have been mainly mapped in these higher wavelengths with the SCUBA camera on the James Clerk Maxwell Telescope.[11]

Synchrotron and cyclotron radiation produce linear and circular polarization, respectively. Perhaps the most interesting source of polarization is the one produced by material around a star. This could be from a protoplanetary disc or a debris disc, a circumstellar disc of dust created by the collisions of planets and minor bodies such as asteroids. As light from the star is scattered by the material in the disk it produces polarization. The degree of polarization depends on the inclination of the disc and the wavelength dependence of polarization gives information on the size of the scatterers. Because the scattering properties of dust are more easily observable than the planets themselves, debris discs provide an indirect means to study planets and planetary formation around other stars. In order to study the atmospheres of a planet, very high sensitivity observations have to be made to separate the small reflected polarized light from the very much larger direct star light.

Some objects are surrounded by geometrically and optically thick torus that prevent us from observing the center object directly with optical and NIR wavelengths. Photon, however, can pass through from the central source and be scattered to us by

dust in the case of stars producing reflection nebulae that can be spatially resolved for galactic sources. Same applies to electrons in Active Galactic Nuclei (AGN). The produced polarization pattern can be used to determine the location of the obscured source, the degree of polarization in the two lobes of the reflection nebula can be used to determine the inclination of the system, and the wavelength dependence of polarization can be used to determine the nature of the scatterers.[11]

Active Galactic Nuclei are the most luminous persistent objects in the universe. The large luminosity is due to the accretion of circumnuclear matter onto supermassive black holes. The energy from AGN is mostly radiated in a form of broad-band continuum emission that can be observed from low-frequency radio to high-energy γ-energies. As AGN are synchrotron sources, they emit linearly polarized radiation. By studying AGN polarization, geometries of magnetic fields and the material distribution in and around the active nuclei can be determined. Degree of linear polarization in AGN are typically around 5% but around 20% has been measured. Even circular polarization has been observed in a handful of sources, with 3C84 being the most notable source with polarization levels up to $\approx 3\%$.[12]

Many stars form a circumstellar shell at the late state of stellar evolution. This is often very difficult to detect as the shell is so close to the bright star. However, in polarized flux the shell can be seen easily. This is because the star, although very bright, has effectively zero polarization, whereas the faint shell has a high degree of polarization and hence relatively high polarized flux.

Although most astronomical observation use linear polarization, circular polarization can also provide many valuable diagnostics. Circular polarization is produced when linearly polarized light is scattered, therefore circular polarization depends not only on the last scatter but also on the prior polarization state of the radiation. Linearly polarized light also morphs into circular polarization when it passes through a medium of aligned grains. These alignments twist along the line of sight converting the Stokes U to Stokes V by birefringence.[11]

5.4 Importance of calibration

In theory the correlation measurements should be simple, but in practice they are not because the radio astronomical receiver system modifies the astronomical polarization. Feeds are almost never perfect thus their polarizations are only approximately linear or circular.

For example in polarimeters with a hybrid, one of the most important contributor to distortions is the electronics system, which introduces gain and phase differences between the two linearly polarized channels. Cables are never truly identical and differ usually in length, which leads to additional phase offset between channels. A difference in gains between the channels leads to a non-zero value for a unpolarized source, making the source appear linearly polarized. If the phases differ then a linearly polarized source appears to be partially circularly polarized. These gains and phases must be calibrated frequently as they can change with time. This is most effectively done by injecting a correlated noise source into both channels.

The hybrid is placed before the amplifiers to simplify the calibration setup, as

now there are only two sets of gains to determine. The problem with this is that the hybrid has loss, and therefore introduces noise.

If the hybrid was placed after the amplifiers, there would be four sets of gains to determine. The correlated calibration signal would have to be on, not only when it is connected to both channels simultaneously but also when it is connected to each one individually, one at a time. Also there is a possibility that if one of the amplifiers is turned off, the whole system seems as it is working properly.

Feeds and electronic devices modify the polarization of the receivers electric field. Generally, a device can couple a fraction of Y voltage into X with an arbitrary phase, and vice-versa. These modification are easiest to describe with the help of Mueller matrix. Mueller matrix relates the output Stokes vector to input Stokes vector:

$$S_{out} = M \cdot S_{in}. \tag{9}$$

As there are four Stokes parameters, Mueller matrix is 4 x 4. To correctly calibrate the system one needs to define the Mueller matrix for the whole system, including the part for sky rotation. After this is done, one simply multiplies the output Stokes vector with the inverse of the system Mueller matrix.

Telescopes also contain unavoidable, intrinsic polarization structures. The fundamental cause of these structures is the curved reflector surface, which slightly varies by the direction of the incident linearly polarized electric vector upon its reflection. On main beam axis these distortions cancel out, but off-axis they do not. Linear and circular polarization react differently to these structures. The distortions increase with curvature, therefore becoming more serious with decreasing focal ratio. As radio telescopes have small f/D, the effect can become very significant.[10]

6 Radio astronomy receivers

This chapter will introduce the basic receivers used in radio astronomy measurements. Also a more recent type of receiver will be introduced in a form of Planck Low Frequency Instrument. This chapter will start with a very simple total power radiometer, going through Dicke receiver and correlation receiver, and finally introducing continuous correlation receiver planned for Metsähovi Radio Observatory.

6.1 Total power radiometer

A radiometer is sensitive receiver that is calibrated to display the brightness temperature. Radiometer must measure precisely the absolute noise power levels. Total power radiometer shown in Figure 2 is a superheterodyne receiver, which intermediate frequency (IF) signal is fed to the detector. First, the thermal radiation received by the antenna is amplified in a low noise amplifier. Then the signal is down-converted to intermediate frequency with a mixer. Typically the mixer is a double sideband mixer (DSB), where both the upper and lower sideband are converted to IF. The noise bandwidth B_n of the IF-amplifier determines the measurement bandwidth. The detector used in radio astronomy is usually of the square law type [15]. The detected signal is integrated to average the noisy output voltage V_{out}.

The output voltage V_{out} includes the DC component that is directly proportional to the system noise temperature and the AC component, that is due to the statistical nature of noise. The DC component can be presented as:

$$V_{dc} = G_s(T_A + T_R), \tag{10}$$

where the T_A is the antenna noise temperature and the T_R is the receiver noise temperature.

The ratio of root mean square (RMS) value of V_{ac} to DC component V_{dc} is $1/\sqrt{B_n\tau}$, where τ is the integration time of the detector output voltage. This is true only if the gain G_s of the radiometer is constant, which is not the case as we will soon see. The sensitivity of a total power radiometer is

$$\Delta T = \frac{T_A + T_R}{\sqrt{B_n\tau}}. \tag{11}$$

A change of ΔT in the antenna temperature at the input produces a change equal to RMS value of V_{ac} at the output.

Slow variation in gain can be eliminated by calibrating the radiometer frequently with loads with a known brightness temperatures. Rapid gain fluctuations deteriorate the sensitivity of the total power radiometer:

$$\Delta T = T_A + T_R\sqrt{\frac{1}{B_n\tau} + (\frac{\Delta G_s}{G_s})^2}, \tag{12}$$

where ΔG_s is the RMS value of the gain fluctuations. In practice the gain stability determines how small a signal can be detected by the total power receiver, but tight temperature control of the radiometer components successfully mitigates these problems[15].[2, 16]

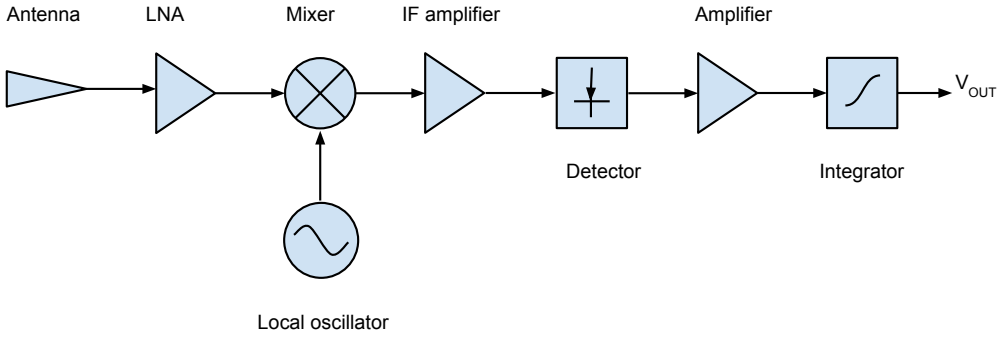

Figure 2: Total power radiometer block diagram.

6.2 Dicke radiometer

In Dicke radiometer the receiver is constantly switched between the antenna and a noise source that has a constant temperature T_c as seen in Figure 3. The output is directly proportional to difference of antenna temperature T_A and the noise source T_c. The switching frequency has to be so high that the gain can be considered constant, in practice 10 - 1000 cycles per second [15].

If the radiometer is balanced, $T_A = T_c$, gain variations have no influence on the output. A Dicke radiometer can be balanced by injecting noise into the antenna branch, by changing the IF gain in sync with the switch generator, or by adjusting the temperature T_c. Because only half of the time is spent measuring the antenna signal and because the final value is an subtraction of two random variables, the minimum detectable noise difference ΔT of the Dicke radiometer is twice of that of the total power radiometer:

$$\Delta T = \frac{2(T_A + T_R)}{\sqrt{B_n \tau}}. \tag{13}$$

[2, 16]

Gain modulation in Dicke receiver can be achieved for example by using two stable passive attenuators. The attenuators are switched synchronously with the input switch into the IF amplifier. If the RF gain of the receiver with the attenuator is denoted as G_A and the signal from the comparison load with the second attenuator as G_C, then the receiver is balanced if

$$(T_A + T_R)G_A = (T_A + T_R)G_C. \tag{14}$$

[15]

When balancing a Dicke receiver with a noise injection, the comparison load is an adjustable noise source. The output noise power of the source is controlled by the receiver-integrator output so that the output is always zero. On VHF (very high frequency) and UHF (Ultra high frequency) frequencies the comparison source can be a noise diode whose anode current is directly proportional to the noise power and can be used as a receiver output signal. At microwave the comparison source could be a fixed output noise generator with a current-controlled attenuator.[15]

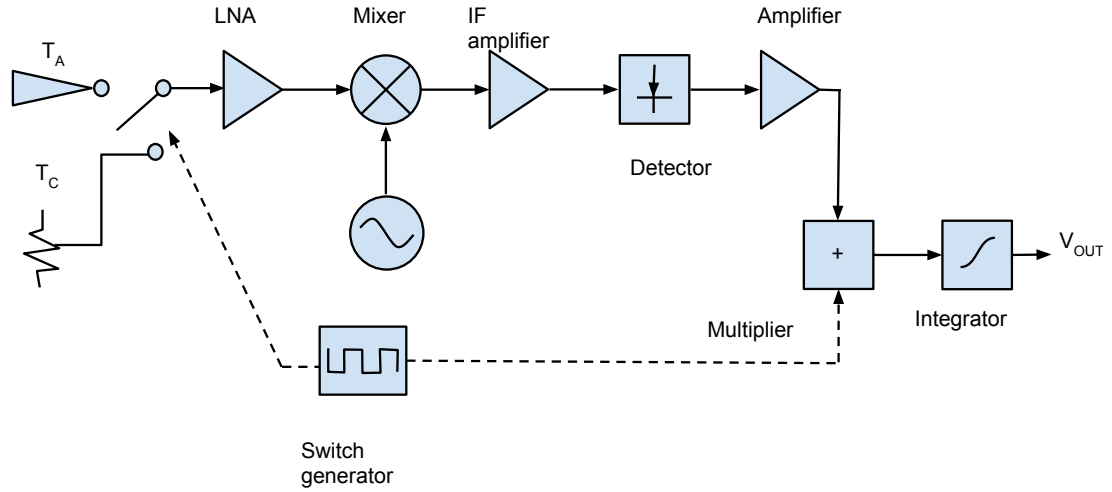

Figure 3: Dicke receiver block diagram.

6.3 Graham's receiver

In regular Dicke receivers the signal power is observed only half of the time. To achieve the full efficiency in observing time, the antenna can be switched between two receivers. If both of these receivers are Dicke type and the outputs are added following the observations, then the sensitivity is increased by a factor of $\sqrt{2}$. These outputs can also be combined electronically during the actual observation as presented by M. H. Graham, seen in Figure 4.[15]

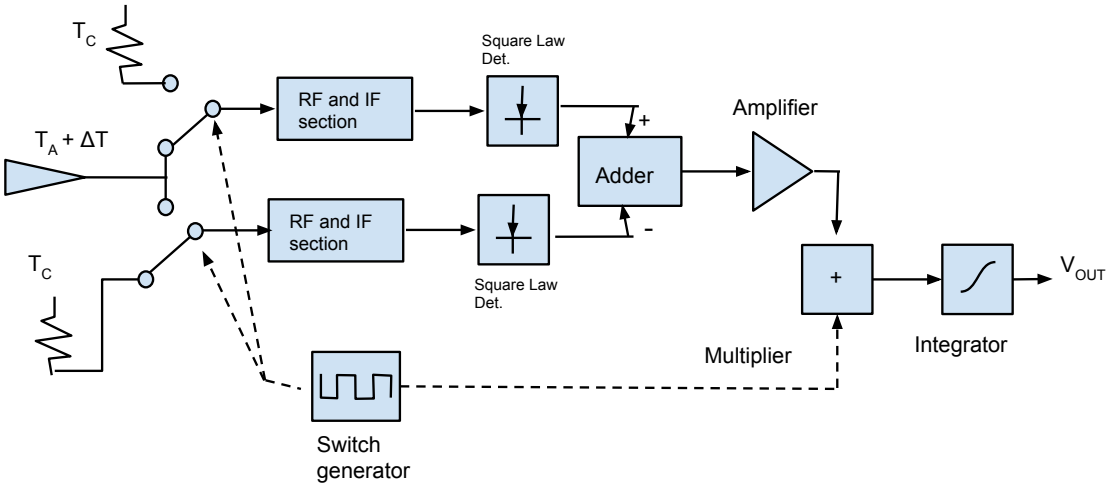

Figure 4: Graham's receiver block diagram.

6.4 Correlation receiver

In correlation type receivers two identical radio astronomy receivers are coupled in parallel to a antenna and the IF-output parts are multiplied as seen in Figure 5. The multiplier output only contains the correlation signal or the signal proportional to the noise power coming from the antenna which is the same for the both receivers. As the noise power from the two receivers are uncorrelated they will not produce a DC output. The sensitivity of a correlation receiver is

$$\Delta T = \sqrt{2}\frac{T}{\sqrt{B_n \tau}}\sqrt{1 + (\frac{\frac{1}{2}T_A}{T})^2}, \tag{15}$$

where $T = (\frac{1}{2}T_A + T_R)$ is the system noise temperature. The detailed calculations can be found in the Appendix part of [15]. If all antenna noise is signal noise then the sensitivity of the correlation receiver is the same as in Graham's receiver. If the receiver noise is small in comparison with the antenna noise and if the signal noise is a small fraction of the antenna noise then the receiver sensitivity is same as in total power receiver. In this case the sensitivity of the correlation receiver in practice will be determined by the gain fluctuations. Therefore, the correlation receiver is useful only when T_A is small.[15]

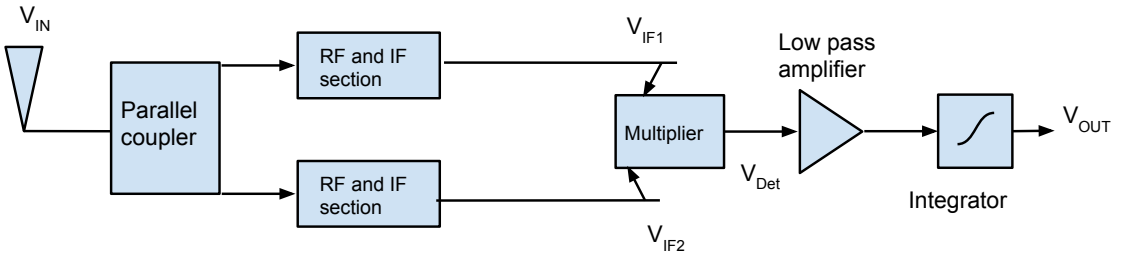

Figure 5: Correlation receiver block diagram.

6.5 Planck LFI

The Planck LFI (Low Frequency Instrument) is an array of radiometric detectors on board the ESA Planck satellite. The receivers use the so called pseudo-correlation scheme with a software balancing technique. The feed horn of the radiometer is connected to an Orthomode transducer (OMT) that separates the incoming radiation into two perpendicular linearly polarized components. Then the sky signal and a stable reference load are coupled to low-noise High Electron Mobility Transistor amplifiers via a 180° hybrid. One of these signals goes through a switch that applies a phase shift which oscillates between 0° and 180° at 4096 Hz. The second signal is

also run through a phase switch for symmetry, but it does not introduce any phase shift. The two signals are recombined in a second 180° hybrid to produce a sequence of signals alternating at twice the phase shift frequency.[17]

In the back-end the RF signals are amplified even further, filtered and then detected. After detection the sky and the reference signals are integrated, digitized and then differenced after multiplication of the reference load signal by gain modulation factor, r, which function is to make the sky-load difference as close to zero as possible. If this difference is zero, or close to it, radiometers sensitivity is given by:

$$\Delta T = \frac{\sqrt{2}(T_A + T_R)}{\sqrt{B_n \tau}}. \tag{16}$$

which is independent of the level of the reference signal. The detailed calculations can be seen in [17].

6.6 New receiver planned for MRO

The new receiver planned for Metsähovi Radio Observatory would consist of 37 - 43 GHz band at beginning and would later add 22 GHz and 86 GHz front-ends. The sensitivity would be a combination of low noise electronics, effective elimination of 1/f noise, and wide bandwidth. The cooled front-end would use state-of-the-art low noise amplifiers (LNAs). The radiometer would be using continuous comparison architecture where signals from the main and reference horns are observed simultaneously. The faint variation of the amplifiers affects only the noise temperature difference of the horns. This noise can be compensated almost completely.

Usually in continuous comparison topology the detection is done directly at the observing frequency. But as continuous comparison method requires the length of the comparison branches to be equal to an accuracy that is proportional to the detection bandwidth, the length difference should be smaller than a fraction of a millimeter. This is why a more practical heterodyne principle is planned. Also the observed band is split into several digitized sub-bands. The pseudo-correlation phase switch is implemented digitally.

The total flux detection and polarimetry follows closely the principle seen in [18]. Equally polarized signal from the two horns are fed through 180° hybrid, which produces sum and difference of the inputs. Then the signal is amplified, mixed down and split into sub-bands and digitized.

The polarization is detected using correlation to compensate the uncorrelated drifts. Stokes V and U parameters are produced by correlating the signals from the orthogonal linear feeds. In order to calculate the Stokes Q, needed for the linear polarization, an additional observation is needed from the other feed that is rotated 45° related to the first one. Thus, the receiver will produce all of the Stokes parameters almost simultaneously. Two observations are needed for linear polarization and the Stokes Q, U, and V are computed using correlation.

The Stokes parameters are calculated with a stack of ROACH2 FPGA boards [19]. Each board processes a 1 GHz sub-band of the total bandwidth. The planned bandwidth is 6 GHz with 6 boards, but this can be increased by adding more

ROACH2 boards. The center frequencies of the sub-bands can be adjusted individually if needed.

The continuous bandwidth is to be split into two 1 GHz bands that are centered at the Metsähovi traditional 37 GHz AGN monitoring frequency and at the VLBI standard frequency at 43 GHz. With 6 GHz of bandwidth and an estimated system temperature of 50 - 80 K, it is expected that sensitivity of 3 mJy (Jy = 10^{-26} $\frac{W}{m^2 \cdot Hz}$), which is required to detect a 2 Jy object with a 0.5% of circular polarization, is achieved in 350 - 900 seconds.

The plan is to build a simulator that can be used to test different design choices and to help with possible problems in the final receiver. Also, a simple room temperature front-end will be built to test and validate the digital correlation before building the cryogenic front-end. This room temperature front-end is the main topic of this thesis, and it will be built for a 22 GHz band.[20]

6.7 Prototype receiver

The block diagram of the prototype receiver is shown in Figure 6. The prototype will use two almost identical antennas that are attached to separate OMTs. The OMT will split the radiation into two orthogonal polarizations. The parallel polarizations are coupled in the hybrid producing the sum and difference of these two signals. The signals are then amplified and mixed to lower frequency. The two signals will be mixed with slightly different local oscillator signals in order to add them to a 500 MHz band that will be fed into the back-end. The back-end will then digitize these signals and produce the Stokes parameters.

The Digital base band converter [21] for VLBI was suppose to be used as the back-end for this prototype. It has a 500 MHz bandwidth and it also limits the IF frequency that could be used. The system turned out have a closed architecture and it works unpredictably. No sensible data could be attained from it, therefore different back-end should be procured. Most reasonable option would be to purchase one ROACH2 board, as those will be needed for the new receiver planned for MRO.

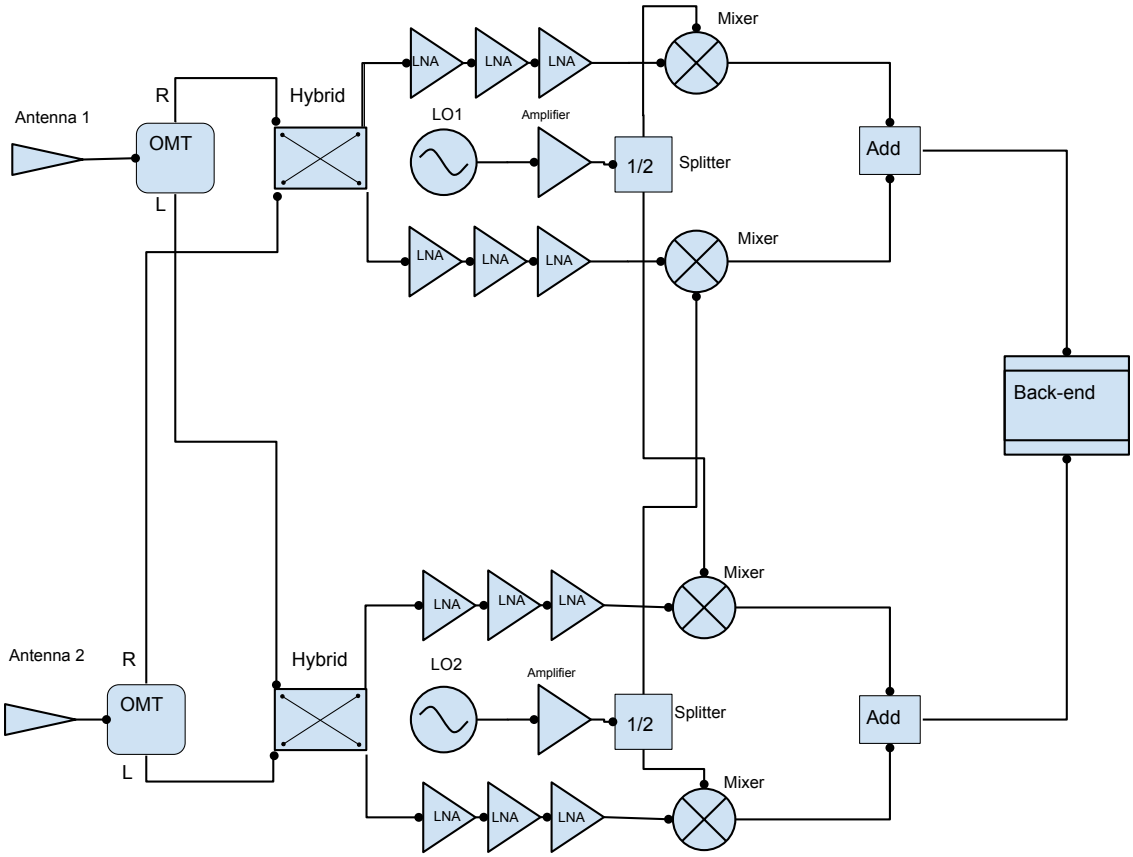

Figure 6: Block diagram of the prototype receiver.

7 Components for the prototype receiver

This chapter will introduce the basic components needed for a receiver. Components for the prototype receiver are also introduced and some justification for their choice is given.

7.1 180° hybrid

The 180° hybrid is a four port device with a 180° phase shift between the two output ports. It can also be operated so that the output ports are in phase. If the signal is applied to port 1, then the signal is split out to port 2 and 3 in phase, and port 4 will be isolated. If the signal is applied to port 4 then the signal is split evenly to port 2 and 3 with a 180° phase shift. The 180° hybrid in this prototype will be used as a combiner. When signal is applied to ports 2 and 3 then the sum of the signals will be formed at port 1, and the difference of the signals will form at port 4. This is why the port 1 and 4 are known as sum and difference ports, respectively.[22] The port placement of the produced 180° hybrids can be seen in figure 7.

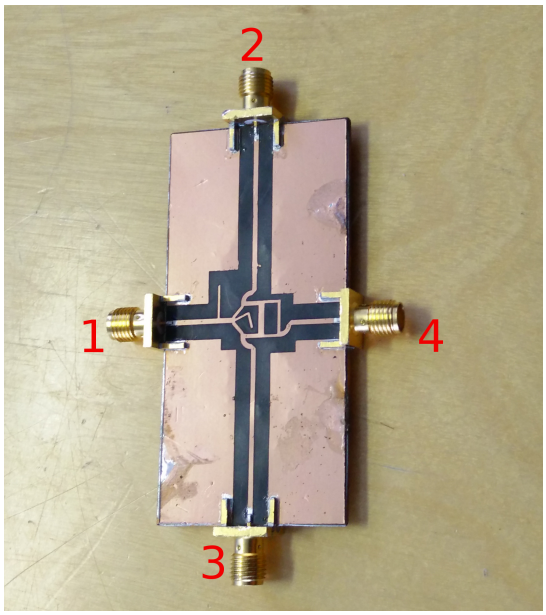

Figure 7: 180° hybrid with labeled ports.

The 180° hybrid for the prototype was produced using planar technology onto a printed circuit board (PCB). The hybrid was suppose to have additional two ports for noise input, but as the noise input was cut from the prototype the additional ports were not needed. The main reasons for choosing PCB hybrid was the low cost and the ease of manufacturing. Although the later one turned out not to be completely true as will be seen in the manufacturing section.

7.2 Mixer

A mixer is three port device that in ideal case produces an output consisting of sum and difference frequencies of the two input signals. The frequency conversion is achieved with a nonlinear or time-varying element. In practical RF and microwave mixers this nonlinear element is either a diode or transistor. As these nonlinear components produce a variety of harmonics and other products of the input frequencies, filtering is needed to select the desired frequency components.

The chosen mixer for the prototype was Hittite HMC571LC5 [23]. It reaches the needed frequency, 22 GHz on the RF and also is suitable for the planned back-end frequencies. Also it is good match for the chosen local oscillator (LO) source as it has an internal frequency doubler. It is small 5 mm x 5 mm surface mountable chip that needed to be soldered onto a PCB with required voltage sources and power filtering. An external 90° hybrid is also needed after the mixer to select the required output from the I/Q mixer.

7.3 Oscillator

In very general term, an oscillator is a nonlinear component that converts DC power to AC waveform. RF and microwave oscillators provide signal sources for frequency conversion and carrier generation. Basic transistor oscillators are usually used in low frequencies, often with crystal resonators to provide improved frequency stability and low noise performance. At higher frequencies, diodes or transistors biased to negative resistance operating point can be used with cavity, transmission line, or dielectric resonators to provide fundamental frequency oscillator up to 100 GHz.[22]

In the few GHz to around 100 GHz range, YIG (Yttrium-Iron-Garnet) oscillators are used in receivers and test devices. YIG oscillators can be tuned by varying an external magnetic field in a wide range. At frequencies higher than 40 GHz, the output from YIG oscillators or commercial frequency synthesizers becomes impractical. Usually higher frequencies are achieved using a lower frequency source that is passed through a nonlinear element, multiplier. In some cases, a series of multipliers is needed to reach the desired frequency.

For frequencies of 100 GHz and higher, Gunn oscillators with a multiplier are used to produce the LO signal. Gunn oscillators are Gallium Arsenide crystals which oscillate when voltage is applied.[6, 22]

7.4 Phase-lock system

The frequency of the LO signal at the mixer must be accurately determined since a varying LO signal will smear the difference frequency. Since the error will grow with the increase in frequency, and the signal may be as much as a few hundreds times higher in frequency than the output of a synthesizer, it is essential to correct the LO frequency. Usually these corrections are carried out with a phase lock loop. The phase lock loop (PLL) system consist of three parts: (1) a voltage controlled oscillator (VCO), which changes the frequency when the input voltage changes,

(2) a phase comparator that produces a signal proportional to the difference of two inputs, and (3) a low pass filter. The inputs for the phase comparator are the reference source and the output from the VCO. Phase detector is sensitive to a small difference frequency. If the phase of this frequency difference varies, an adjustment is applied to the current source of the oscillator. This will force the frequency of the oscillator to change in a way that brings the LO frequency closer to the desired value. The phase difference is said to be stable, when the LO is locked to the reference frequency. If a system is phase locked, it is also frequency locked.[6]

7.5 Local oscillator for the prototype

Evaluation board EV-ADF5355SD1Z [24] from Analog Devices was chosen as the local oscillator source for the prototype. The evaluation board is a self-contained package including PLL, VCO, loop filter, USB interface, and voltage regulators. The board contains the ADF5355 [25], a microwave wideband synthesizer with integrated VCO, that provides a RF output frequency range from 54 MHz to 13600 MHz.

Two resistors were removed from the evaluation board according to the data sheet. The first removal disabled the internal LO and the second enabled the use of single mode external oscillator signal. The evaluation board itself doesn't put out enough power for the chosen mixer, therefore at least one amplifier needs to be added before feeding the signal into the mixer. Spare amplifiers available at Metsähovi were used.

7.6 Low noise amplifier

Low noise amplifier amplifies the low-power signal without increasing the signal-to-noise ratio (S/N) substantially. This low noise factor comes usually with the price of the gain.

The HMC751LC4 [26] from Hittite Microwave Corporation was chosen as the LNA for the prototype receiver. HMC751LC4 is a 4 mm x 4 mm surface mountable chip that was soldered onto the the same PCB as the mixer. The LNA was fitted with its own voltage regulator and power filtering. The LNA has noise figure of 2.2 dB and a gain of 25 dB. It was chosen due to its price, high gain and frequency range of 17 - 27 GHz. As the signal from astronomical sources if very low, three consecutive LNAs was planned, with some tunable attenuation in between the amplifiers. The attenuation was done in the form of a π-pad. It is an attenuator circuit, in which three resistors are placed between the amplifiers forming a π-shape. As the transmission lines are very narrow, the resistors will be surface-mount device (SMD) type instead of through-hole components.

7.7 Power supply

Adjustable power supplies were used to power on the system. The input power was adjusted by MCP1824 [27] regulators from Microchip. Amplifiers needed a current around 70 mA and a voltage of 4 V whereas the mixer needed current of 120 mA

and a voltage of 3.5 V. To keep the component quantity low, ready available resistor values were used and the final voltage for the amplifiers ended up as 3.96 V and voltage for the mixer was 3.56 V.

7.8 Antenna choice

Metsähovi had couple of spare horn antennas available: one corrugated antenna and two twisted pyramid antennas. But as we needed two identical antennas only the twisted pyramid antennas could be chosen. The corrugated horn would have resulted in more gain, but as the budget was so small, producing a copy of the corrugated antenna was not possible, and manufacturing a identical copy of the first one would have been more time consuming than just ordering two new ones. The twisted pyramid antennas had a slightly different mounting pieces and one of the antennas had been lengthened afterwards, which meant that they were not of the same length. Due to the small budget, it would have to do and the difference would have to be compensated in simulations and calculations.

A rough estimation for the gain of the antenna was calculated using equation for a horn antenna gain:

$$G = \frac{4\pi A}{\sqrt{\lambda}} e_A. \tag{17}$$

The A is the physical area of the aperture, λ is the wavelength, and e_A is the aperture efficiency, a figure between 0 and 1. With the area being 13.5 cm^2 and the aperture efficiency estimated as 0.5, the antenna has an estimated gain of 27.9 dB at the frequency of 22 GHz.

7.9 Orthomode transducer

Orthomode transducer is a component that separates or combines two orthogonally polarized signal paths. Though the final receiver would use circularly polarization orthomode transducers (OMTs), a linearly polarizing OMT was chosen due to the cost benefits. Due to its intriguing design and ease of manufacturing the design presented in [28] was selected for the OMT. This orthomode transducer consist of orthogonal balanced coaxial probes in a 11.557 mm (0.455 inches) diameter circular waveguide linked by coaxial transmission lines to balanced coaxial probes in orthogonal WR-42 waveguides. The design used the parameters reported in [28], with couple of modification due to misprint in the original paper. Also some of the parameters were modified to ease the fabrication.

The OMT consist of two aluminium block that were fabricated with standard end-mill, a coaxial transmission lines inserted inside the block and two WR-42 waveguides inserted inside the output ports of the aluminium block. The OMT is held together with four M3 bolts. The antenna and output adapters are each attached with four M3 bolts.

8 Design and manufacturing of the 180° hybrid

Due to budgetary reasons, cost became the prominent factor in the design process. As the budget was around the price of one decent waveguide OMT, most of the components had to be built in-house or use spare parts available. This is why the 180° hybrid was chosen to be manufactured as microstrip. This chapter will first show the design and manufacturing process of the hybrid. After that, the iterating phase and testing results are presented.

8.1 Hybrid design process

A variety of different empty printed circuit boards (PCBs) were available at Metsähovi. As the prototype was design for K-band (18 - 26 GHz), FR4 was not a viable option due to high losses on frequencies over 1 GHz [29]. Rogers 5880 was chosen as the primary board material after some simulations with CST MICROWAVE STUDIO [30]. The problem with Rogers 5880 was that many companies won't even try to manufacture PCBs using the aforementioned material. This meant that everything had to be done in-house using commercial off-the-shelf (COTS) equipment and chemicals. This included the masking and the etching process and everything that those processes involved. After brief prototyping Rogers 4350B was also considered as then the manufacturing of the PCBs could be outsourced to private companies. The Rogers 4350B board would have large losses, which are critical as the hybrid is placed before any amplification, but on the other hand due to the accuracy needed for the line widths and lengths it might be a better choice.

The hybrid design in [31] was used as a starting point for the 180° coupler. Using the impedances optimized in the [31], the needed lengths and widths for different substrates were calculated using AWR's TX-LINE [32] tool by National Instruments. For each different substrate a couple of different substrate heights were also calculated. The primary focus was on the material that were available in Metsähovi, which included mainly Rogers Duroid 5880, 5870 and 6010. Each of which had a couple of different substrate heights. For each group of lengths and widths, also the angles between the different microstrip needed to be designed as the whole pattern doesn't grow isotropically with increase of frequency or the change of dielectric constant of the substrate.

As the coupler in the paper was design to work around 10 GHz frequencies, the design was first confirmed to scale up to the wanted K-band. According to AWR's Microwave Studio the design would scale well to the higher frequencies, but AWR takes into account only part as individuals and doesn't consider their coupling. Therefore a more detailed simulations were needed.

Using the preliminary lengths, widths and angles calculated in AWR, a more detailed model was produced in CST MICROWAVE STUDIO [30]. Mainly the lengths and the angle of microstrips were fine tuned to make the pattern whole. Once the pattern was whole, the system was simulated using Transient solver.

The final design comprised of many microstrip parts, which meant that individually optimizing each strip would have been very time consuming. Therefore

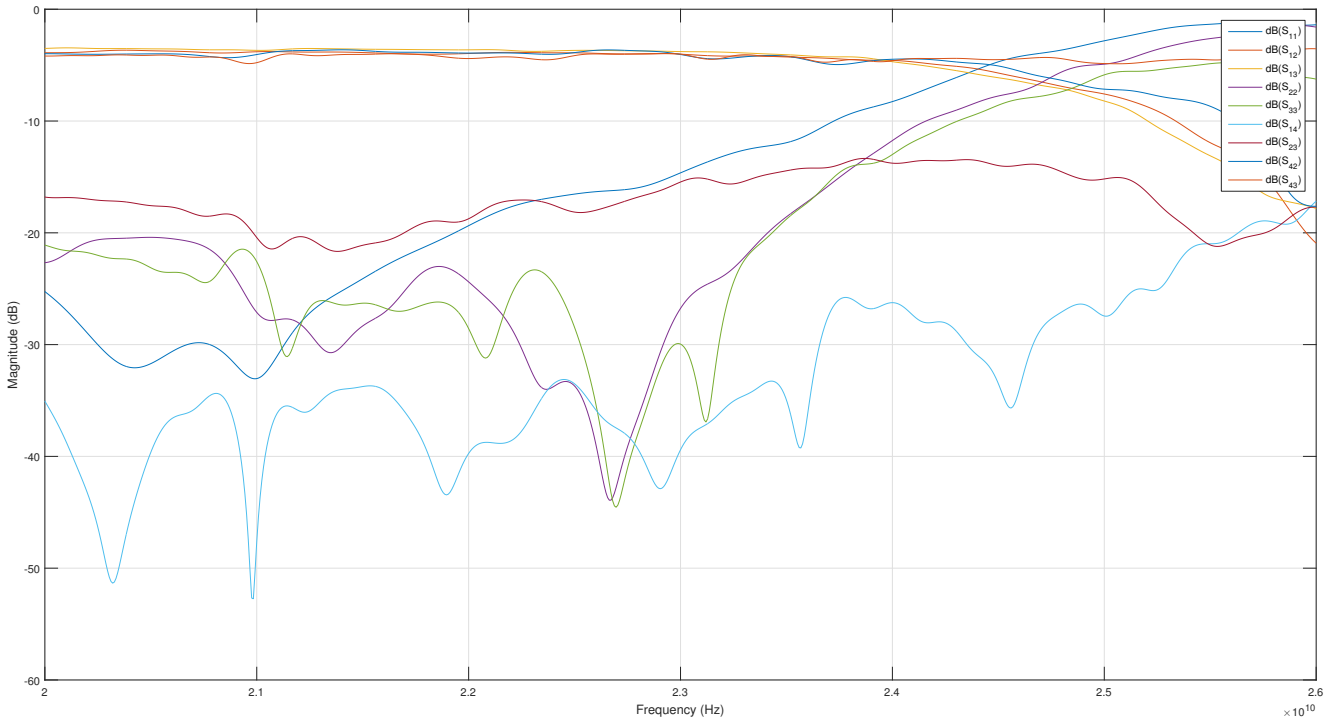

Figure 8: Simulated S-parameters for Rogers 5880 h=254 μm with copper thickness of 35 μm.

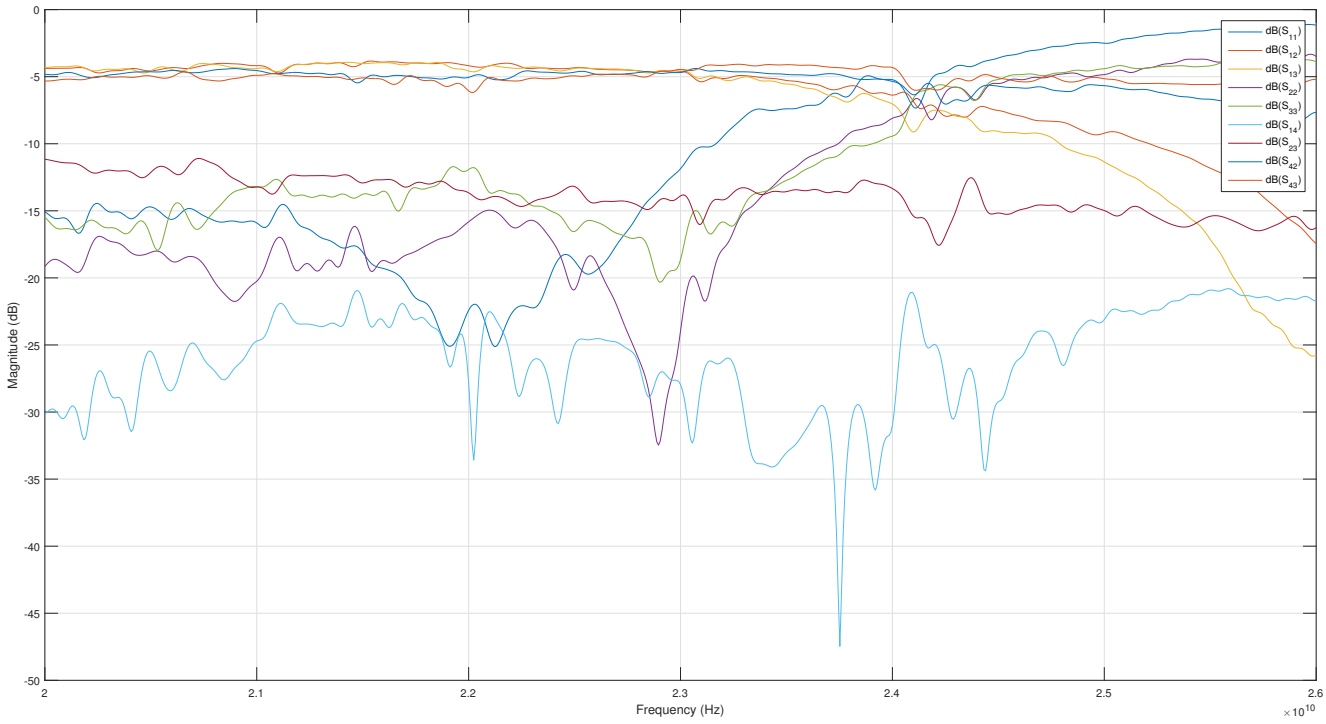

Figure 9: Simulated S-parameters for Rogers 6010 h=254 μm with copper thickness of 35 μm.

optimization was concentrated on the angle between striplines and the height of the substrate. After multiple simulations two promising group of parameters was found for Rogers 5880 and 6010. Both of which had the height of 0.254 mm. The simulated S-parameters for the coupler on Rogers 5880 and 6010 can be seen in Figure 8 and 9, respectively. Rogers 4350B was kept in mind as this material was available in couple of fabrication companies. However, the simulations on Rogers 4350B were not very encouraging, as can be seen in the S-parameters shown in Figure 10. This meant that the coupler would have to be produced in-house.

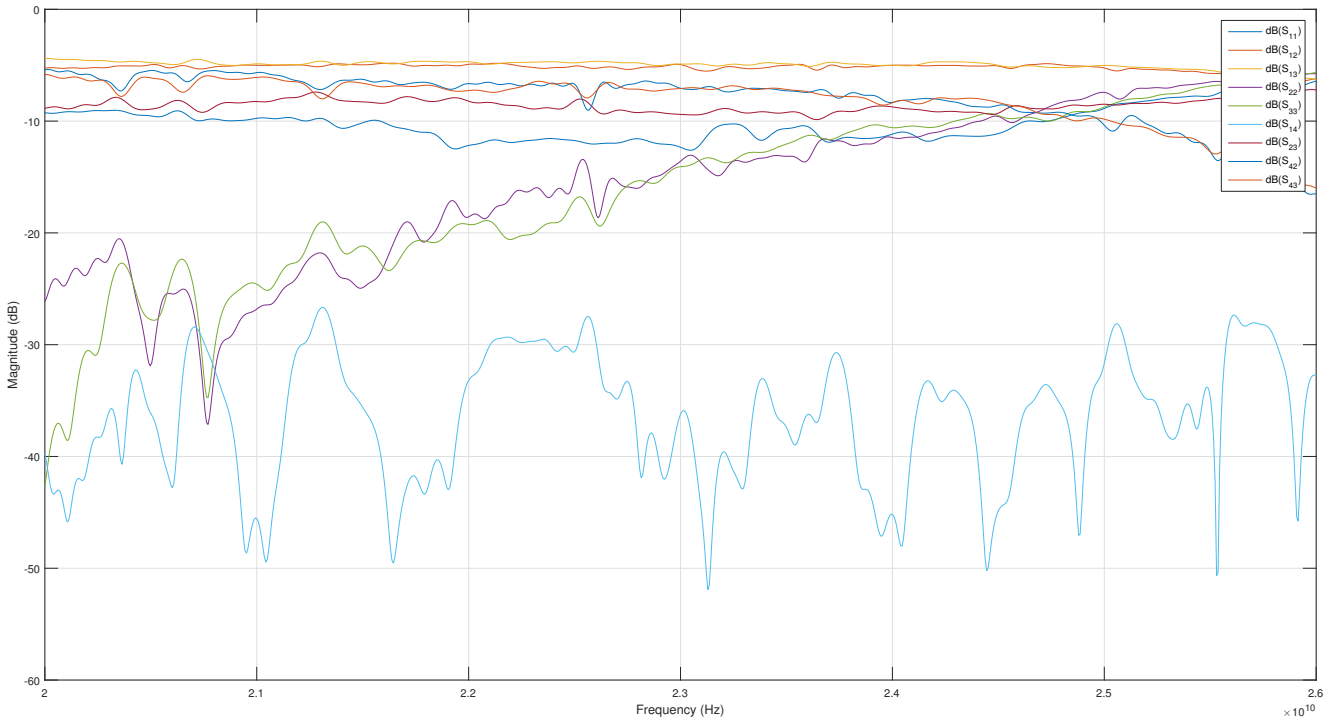

Figure 10: Simulated S-parameters for Rogers 4350B h=254 μm with copper thickness of 35 μm.

If the working band is defined so that the $S11$ has to be below 15 dB, then the simulated Rogers 5880 has a bandwidth of over 2.95 GHz (20 - 22.95 GHz). The ideal hybrid splits the signal into two, so with a 3 dB loss. The simulated Rogers 5880 has an $S42$ ranging from -3.63 dB to -4.05 dB and an $S43$ ranging from -3.96 dB to -4.83 dB on the previously stated bandwidth. The simulated hybrid from Rogers 6010 has a bandwidth of 1.65 GHz (21.16 - 22.81 GHz). The channel split is also worse with $S42$ ranging from -4.60 dB to -5.46 dB and $S43$ ranging from -4.80 dB to -6.18 dB. The simulated hybrid from Rogers 4350B had a $S11$ of only -12.6 dB at the lowest. Therefore, Rogers 4350B was discarded from further simulations.

8.2 Manufacturing the 180° hybrid

To create the etching mask onto the PCB, first the so called ironing technique was used. In this technique the wanted pattern is printed onto a paper with a laser printer. The paper with the pattern is then placed on top of the PCB and ironed with a regular flat iron for around 5 minutes constantly applying pressure to the board. After this the board with the paper still attached to it is soaked in cold water for several minutes until the paper could be easily removed leaving only the masked pattern. Finally, ferric chloride ($FeCl_3$) is used as etchant to remove the unwanted copper i.e. everything not covered by the mask.

Making PCBs with regular paper resulted in uneven finish and the lines where almost never complete. Using projector sheets and glossy photo paper resulted in more even lines but still not all of the toner transferred to the board. By far the best result came with Press and Peel films that are designed for transferring patterns to PCB. The lines were still some what uneven due to the toner transferring to a different degree. Uneven surface and temperature gradient of the flat iron is probably the main reason for this. There were couple of tries that resulted in satisfactory enough pattern that they were manufactured further.

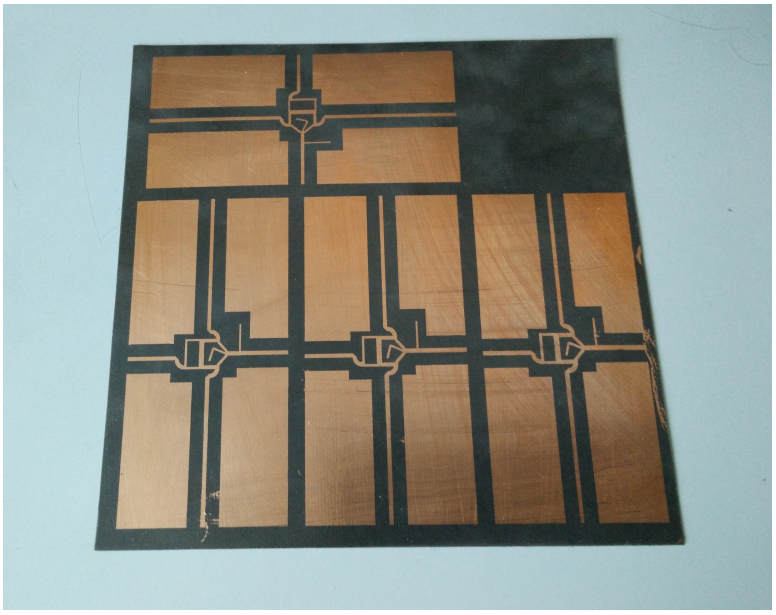

Figure 11: Etched hybrid board resulting from the UV-lighting technique.

As the result from the ironing technique were mostly unsatisfactory, UV-lighting technique was also used to produce a hybrid. In this technique a thin layer of liquid photo-resist is applied onto a clean copper surface. Once it has dried, the circuit layout is printed onto a transparent paper and placed on top of the circuit. Then the whole board is exposed to UV-light. The exposed resist can then be removed by developing the board in a sodium hydroxide (NaOH) bath. The excess copper is wet-etched with ferric chloride leaving the wanted circuit pattern behind. Finally

the resist on top of the circuit is removed using acetone (C_3H_6O). The resulting board can be seen in Figure 11.

The UV-lighting technique resulted in lines that were more even and precise compared to the ironing technique, but were still not perfect. The UV-lighting technique produced the mask more close to the wanted pattern and no clear holes where present. Still the resulting microstrip lines where not the correct width due over- and under-exposure but they would suffice. Some of the copper lines were thinner than in the design due to etchant interacting better on some areas than others. Also the lines were not rectangular or the walls of the copper vertical due to wet etching working isotropically. This means that the etching rate is the same in both horizontal and vertical direction, which will leave the copper edges looking similar to what is illustrated in the Figure 12.

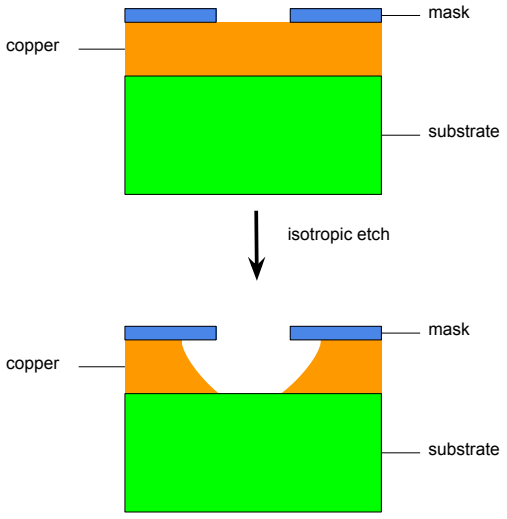

Figure 12: Isotropic etching process.

8.3 Iterating and testing the 180° hybrid

First tested PCB board was made from Rogers 5880 but the result were very unsatisfactory. Signal power loss was around 50 dB and the smallest loss was from port 4 to port 1 which should have the largest isolation.

The second hybrid produced looked more promising but due to some scaling issues the band was not were we needed it to be. The incorrect scaling occurred during the mask manufacturing process as the automatic scaling was left on during the printing of the mask. The resulting coupler did prove that the design of the hybrid was plausible.

After some iterations a coupler with a good phase balance was fabricated, however, the amplitude characteristics were poor, as can be seen in Figure 13. The root

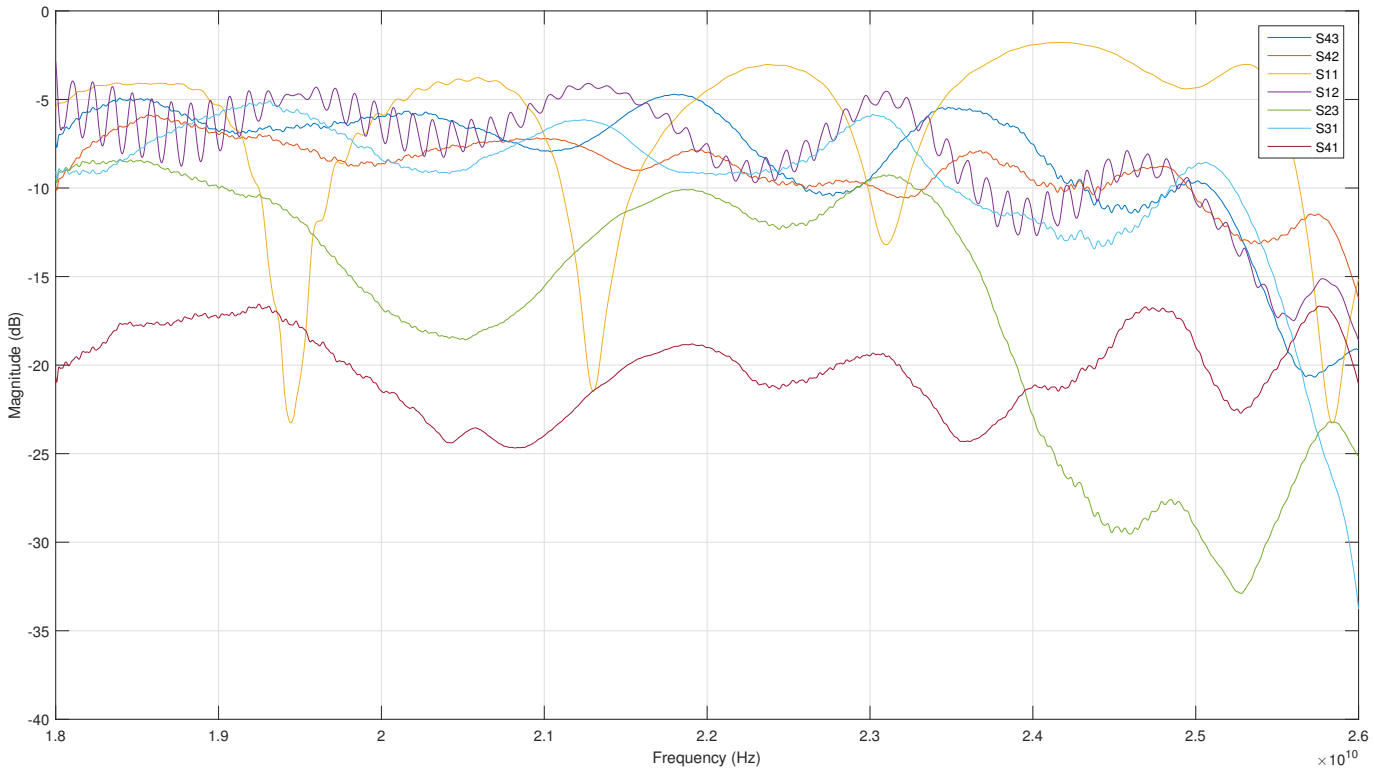

Figure 13: The S-parameters of a early prototype made from Rogers 5880, h=254 μm with copper thickness of 35 μm.

of the problem was the improper grounding of the end-connector SMAs. The board was only 0.254 mm thick were as the SMA connectors rods had a spacing of 1.57 mm. This gap would expose the hybrid to large stress and tension due to measuring cables. In an earlier hybrid, an improvement of 10 dB in the $S21$ parameter could be achieved only by soldering the ground connection properly. This meant that the hybrid had to be mounted onto a rigid plate and the ground connection had to be solid.

Aluminium was considered for the structural support, but soldering to it would be difficult with the tools available. A regular double sided FR4 PCB was therefore chosen. As the FR4 needed to be soldered to the Rogers Duroid board but still have a ground pins of the SMA connector soldered to the original ground plate on Rogers Duroid board, soldering was difficult and formed a bulk in the Rogers board.

Iron plate was also considered and tested as soldering would be easier and the plate and the Rogers Duroid boards could be just glued with a conductive epoxy to produce solid ground plate. The amplitude characteristics and the phase response of the iron-plated couplers were unsatisfactory. The SMA connections were thought as the main reason for these results, but also the parasitic properties of the magnetic iron plate were considered.

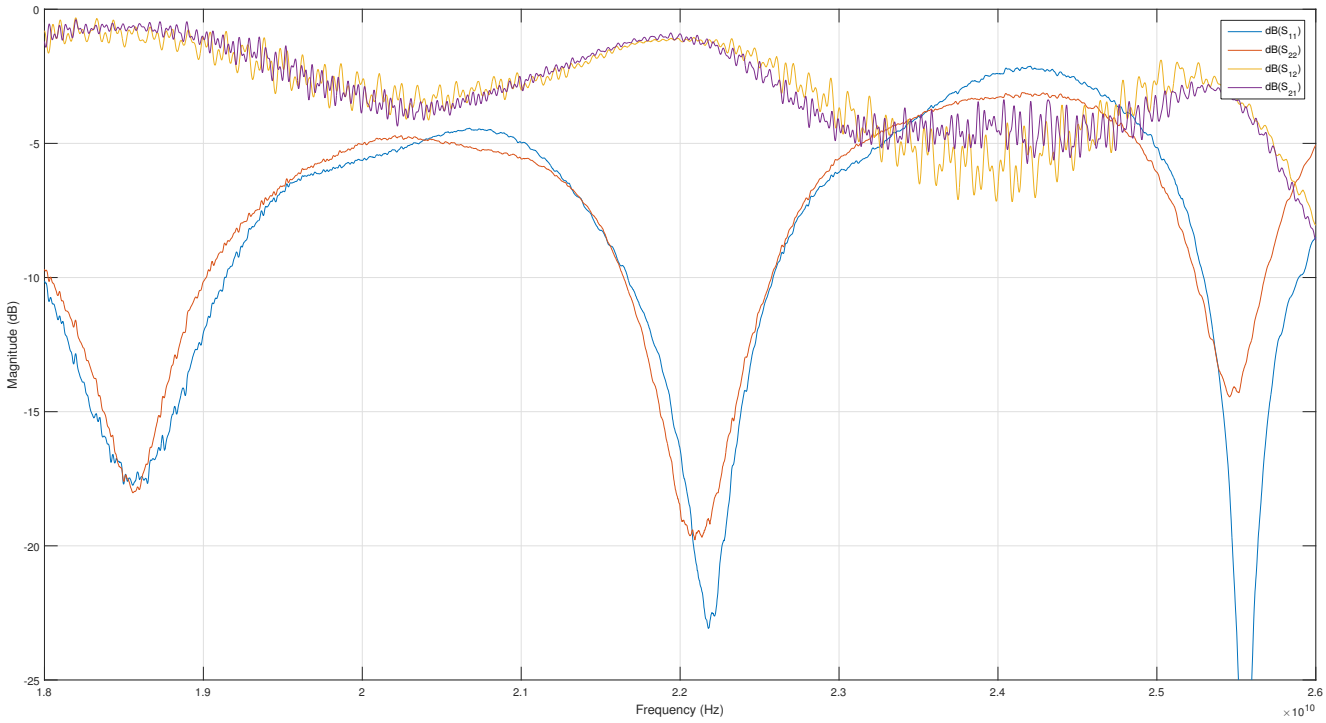

Figure 14: The S-parameters of a long through piece made from Rogers 5880, h=254 μm copper 35 μm.

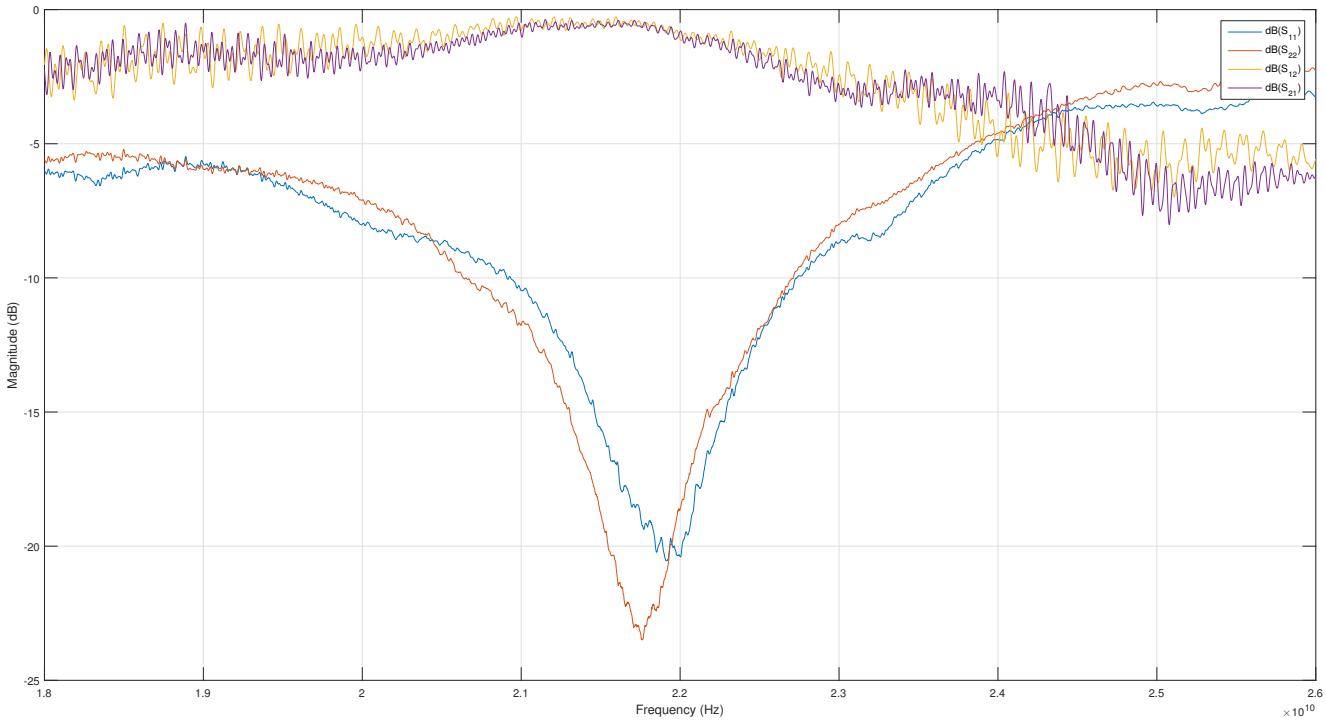

Figure 15: The S-parameters of a short through piece made from Rogers 5880, h=254 μm copper 35 μm.

To solve the loss in the Rogers material per length, two different length through pieces were produced. Both through pieces had 1 dB loss at 22.0 GHz as can be seen in Figures 14 and 15. Although the losses per length couldn't be determined, it was clear that the soldering of the input ports is very important and can produce uneven signal paths in the system. It also shows that the SMA adapters can still work at these higher frequencies.

The best hybrid pair produced was from the Rogers 5880 with a 35 μm thick copper plating named simply as H and G. Detailed measurements were done with Agilent E8363A PNA series network analyzer with a measuring capability from 45 MHz to 40 GHz. The S-parameters and phase-response of the hybrid H can be seen in Figures 19 and 20, respectively. The hybrid G's S-parameters and phase-response can be seen in Figures 17 and 18, respectively. Although they were not identical and the amplitude response was a still unsatisfactory, they could suffice in this prototype phase. The problem with the hybrids G and H was that they were very flexible and would therefore endure torque produced by the measuring cables.

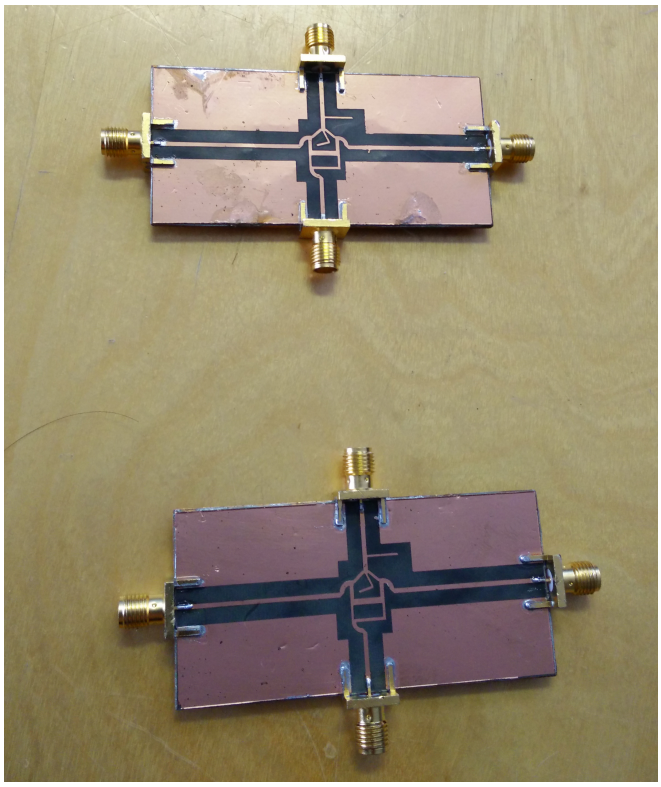

Figure 16: Copper plated hybrids I and J.

A more structurally solid version of these hybrid was manufactured by soldering a pure copper plate under the PCB. This resulted in hybrids I and J, which can be seen in the Figure 16. Their S-parameters and phase responses can be found in Figures 21, 22, 23, and 24. As can be seen, their responses are not as good as in hybrids G and H but their structural design would endure better the tensions and moments occurring during testing.

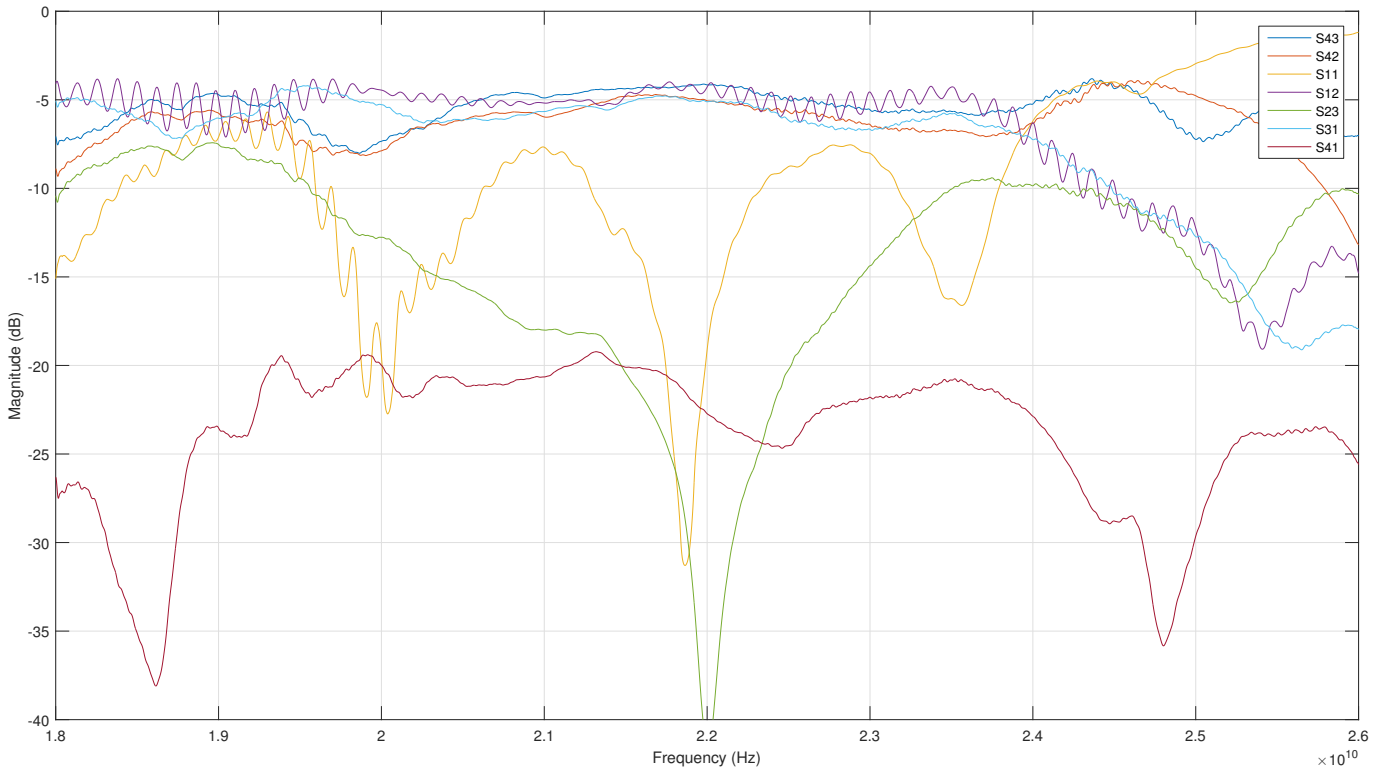

Figure 17: The S-parameters of hybrid G made from Rogers 5880, h=254 μm, copper thickness 35 μm.

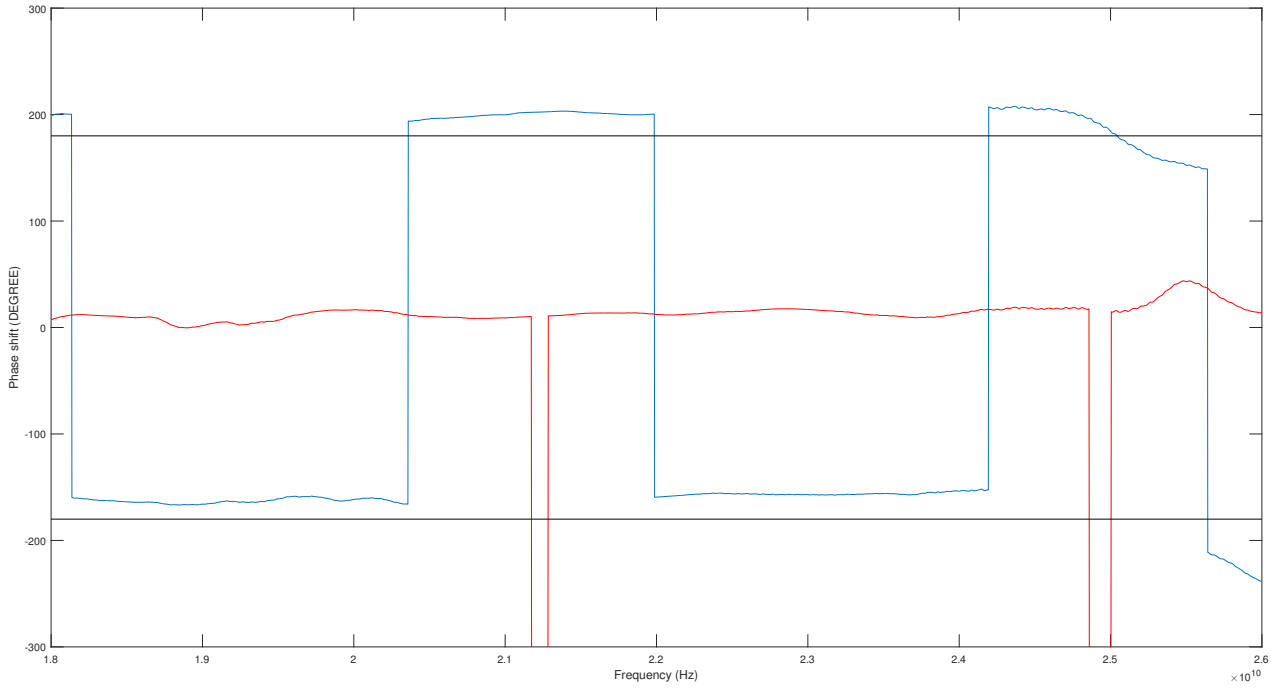

Figure 18: The phase response of the hybrid G's delta port.

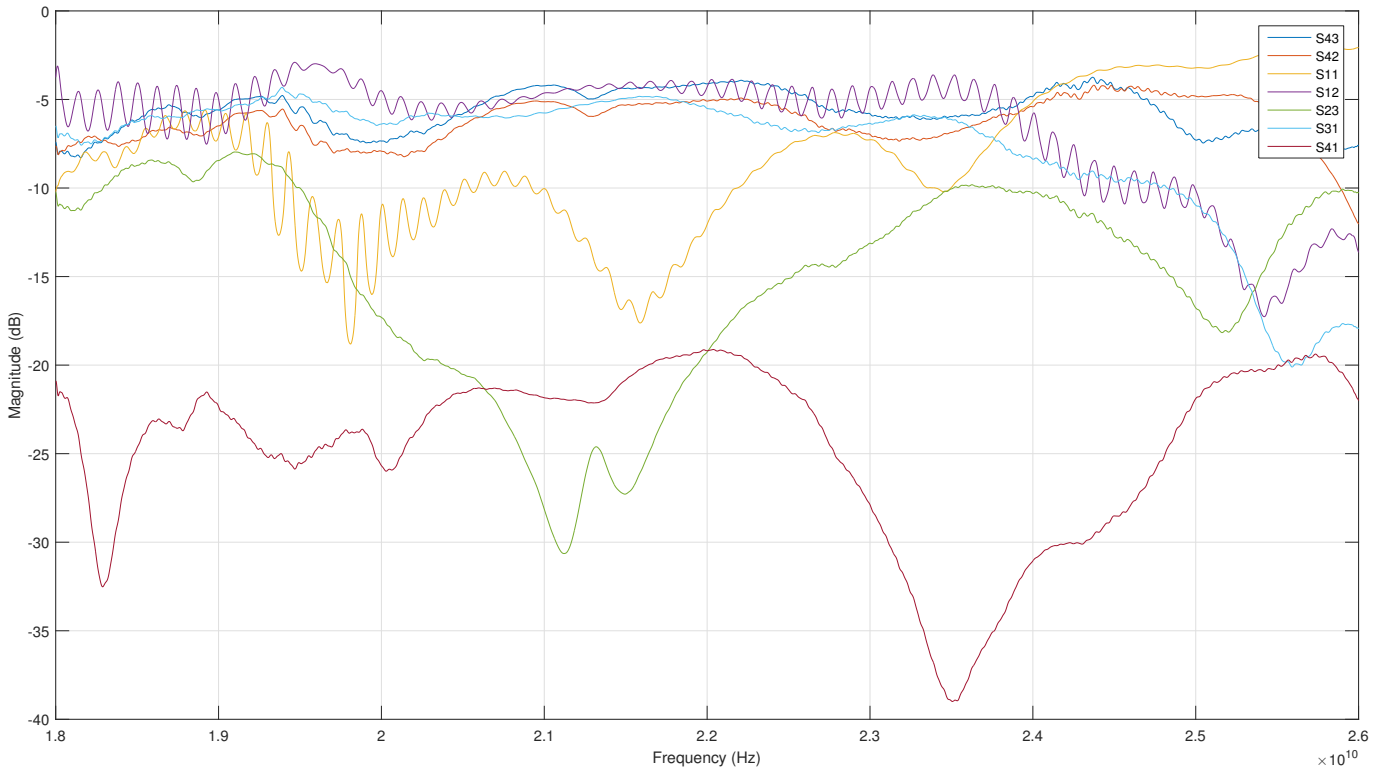

Figure 19: The S-parameters of hybrid H made from Rogers 5880, h=254 μm, copper thickness 35 μm.

The manufactured hybrids have much tighter matching compared to the simulated ones. For example the hybrid I has a bandwidth of 260 MHz (21.80 - 22.06 GHz) where the $S11$ is below 15 dB. There are also some other bands that have low enough $S11$ but those are not close enough to the wanted frequency of 22 GHz. Also the coupler split is worse with $S42$ peaking at -7.56 dB and $S43$ measuring -6.89 dB at best. The hybrid H had a similarly limited bandwidth of 350 MHz (21.41 GHz - 21.76 GHz) but it didn't quite reach the wanted frequency. It does have a bit more satisfying signal split with an $S42$ from -4.29 dB to -4.55 dB and an $S43$ from -5.8 dB to -5.54 dB on the previously stated frequency range.

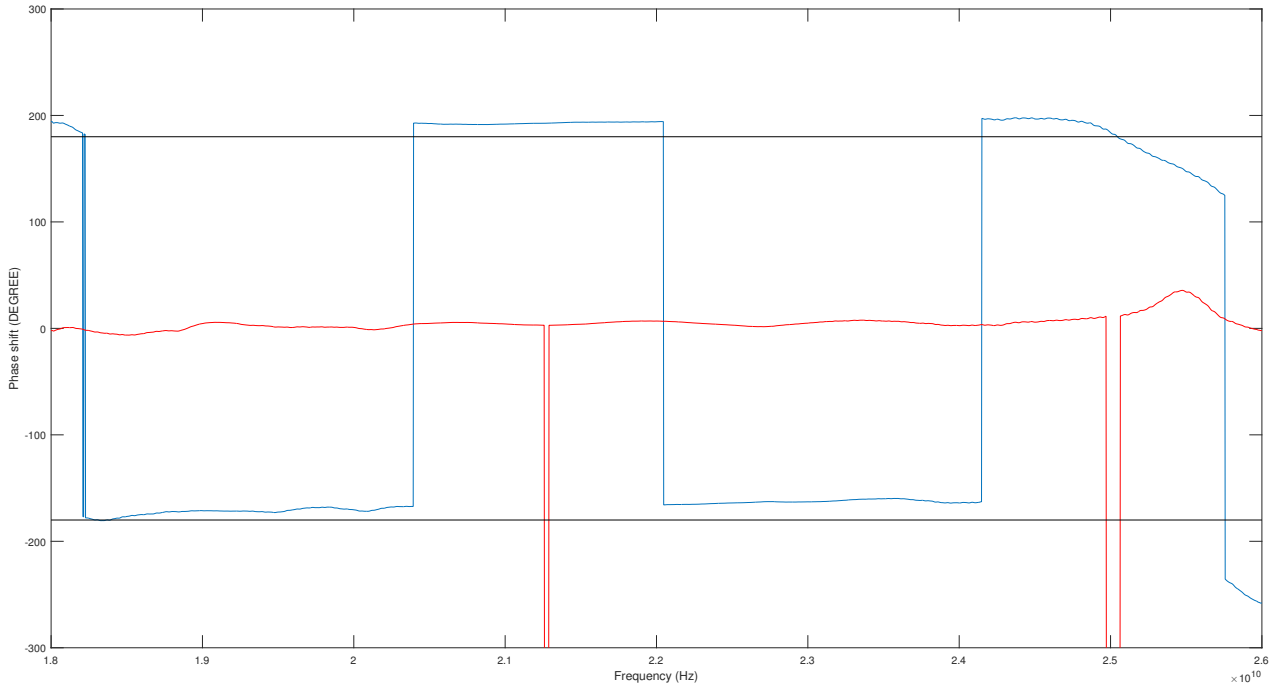

Figure 20: The phase response of the hybrid H's delta port.

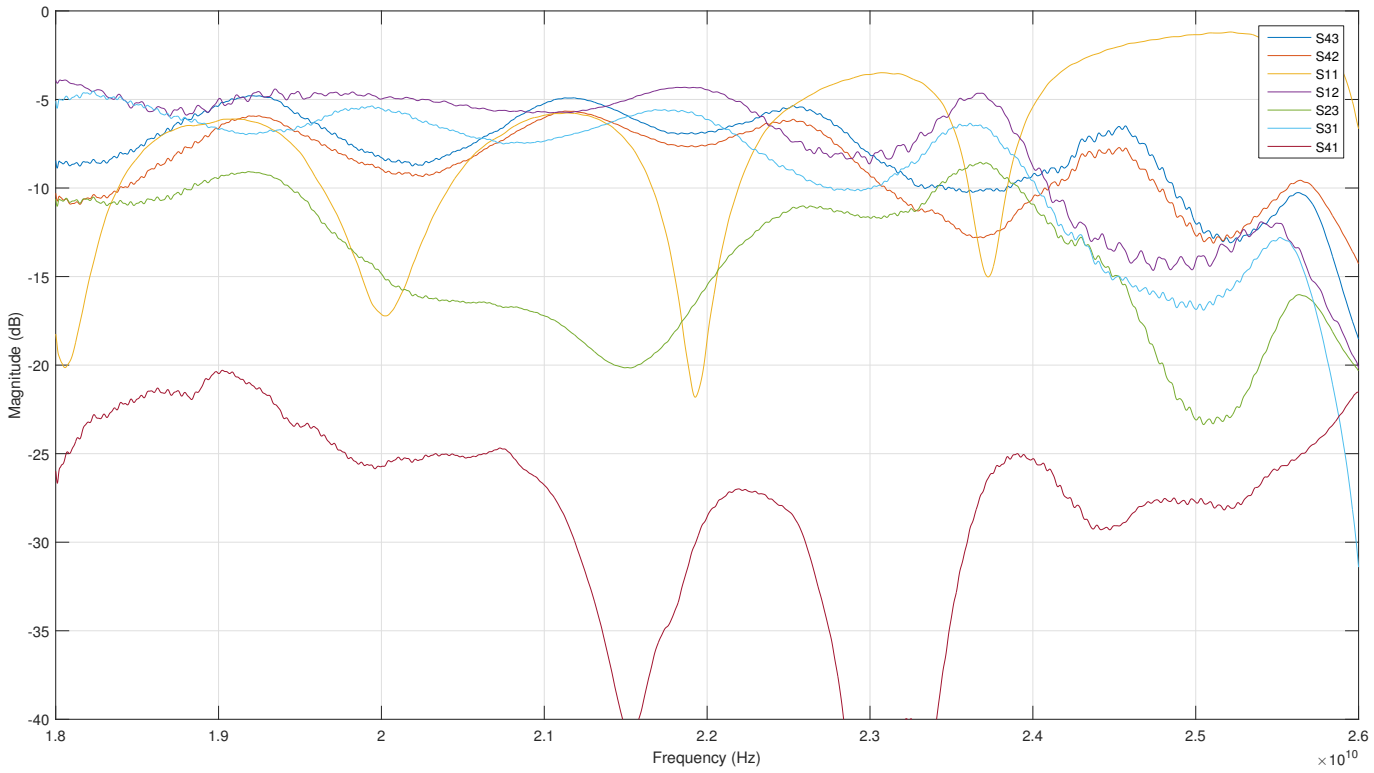

Figure 21: The S-parameters of hybrid I made from Rogers 5880, h=254 μm, copper thickness 35 μm.

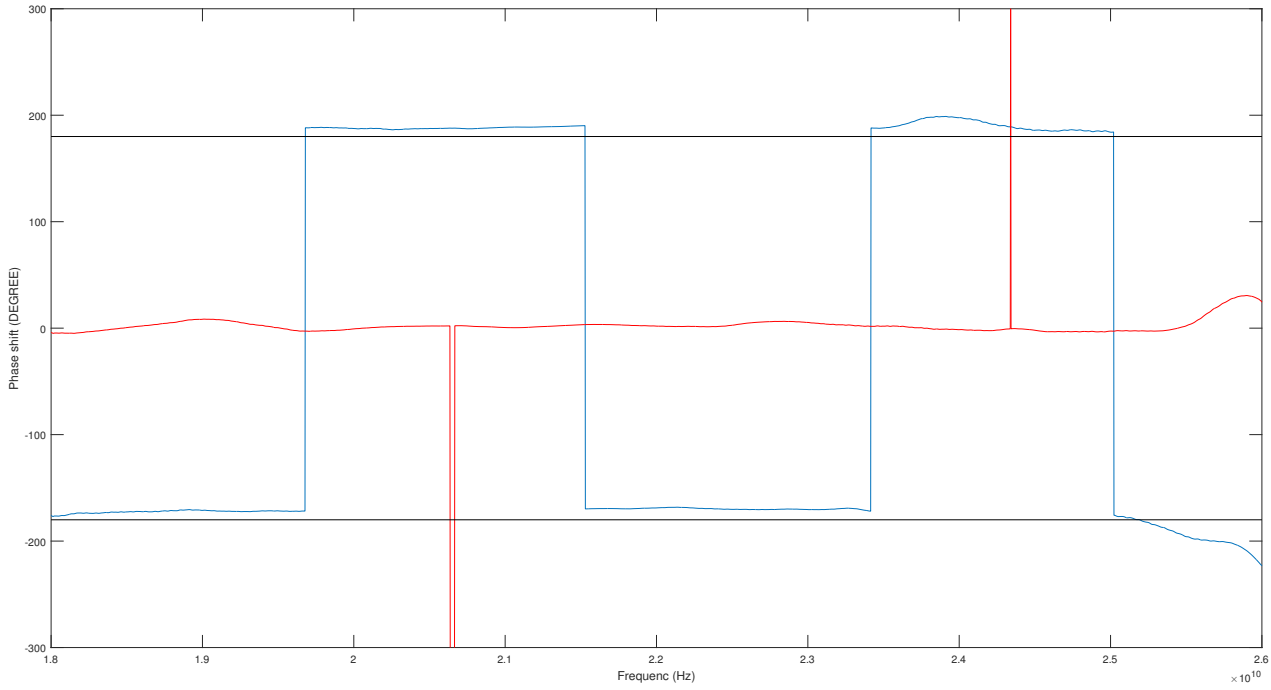

Figure 22: The phase response of the hybrid I's delta port.

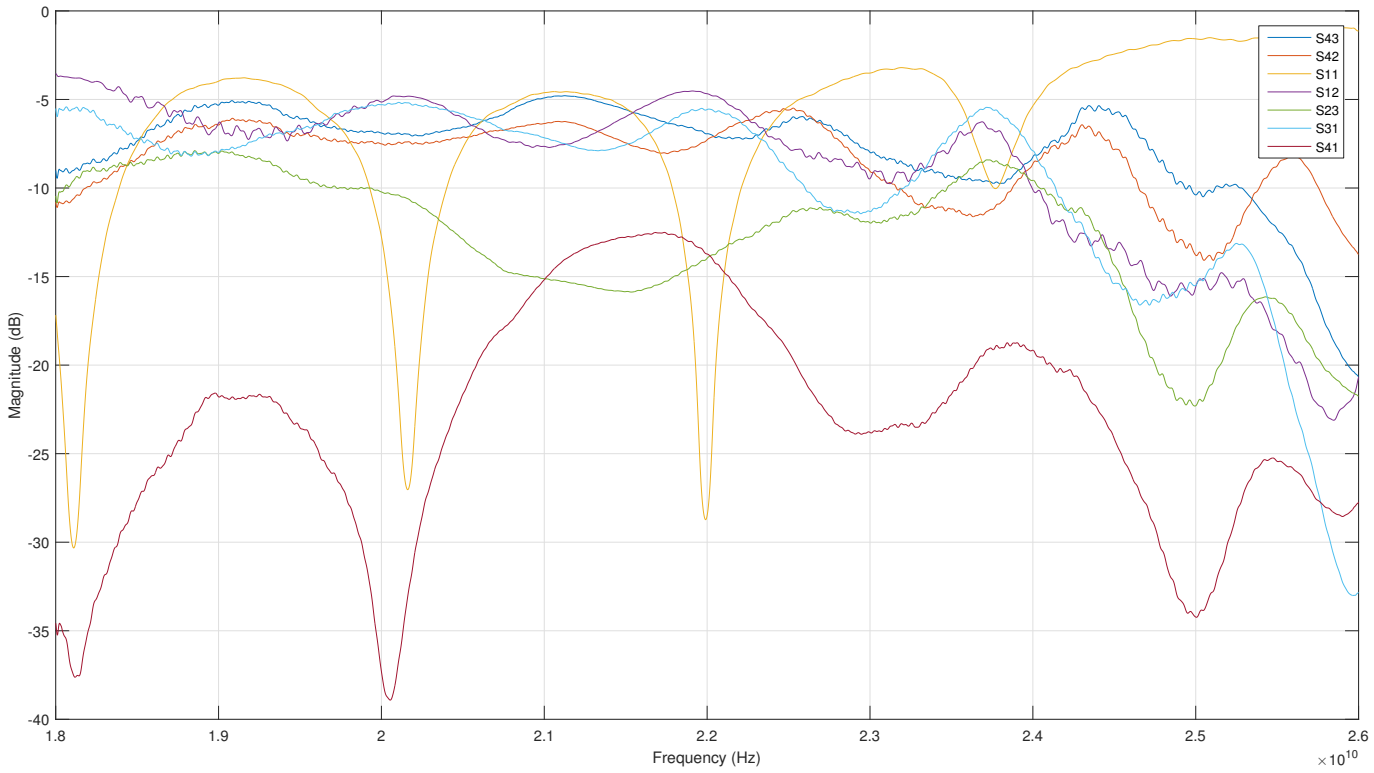

Figure 23: The S-parameters of hybrid J made from Rogers 5880, h=254 μm, copper thickness 35 μm.

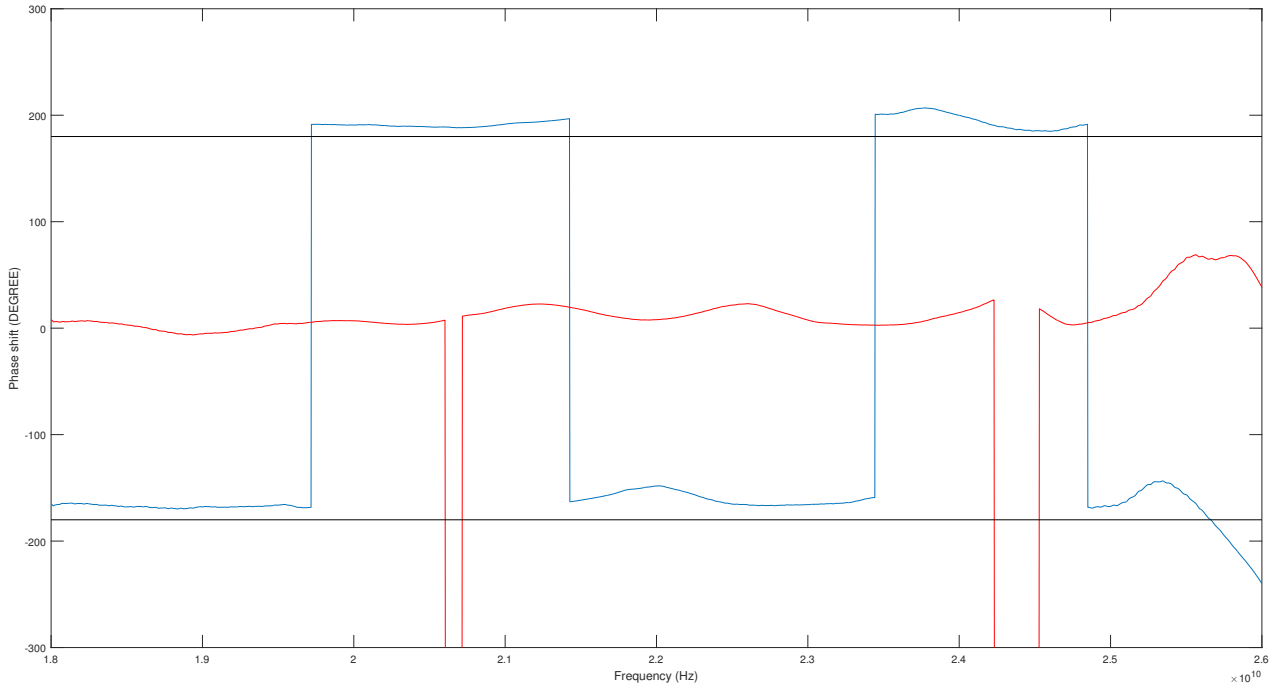

Figure 24: The phase response of the hybrid J's delta port.

9 Orthomode transducer for the prototype

9.1 OMT assembly

The aluminium blocks for the OMT were manufactured by Precia [33]. They still needed to be fit with rectangular waveguides and transmission lines to finish the OMTs. This was done at MRO. The transmission lines were made from coaxial cable and needed to be bent to a proper form before inserting them into the OMT. The open OMT with fitted transmission lines and waveguides can be seen in Figure 25.

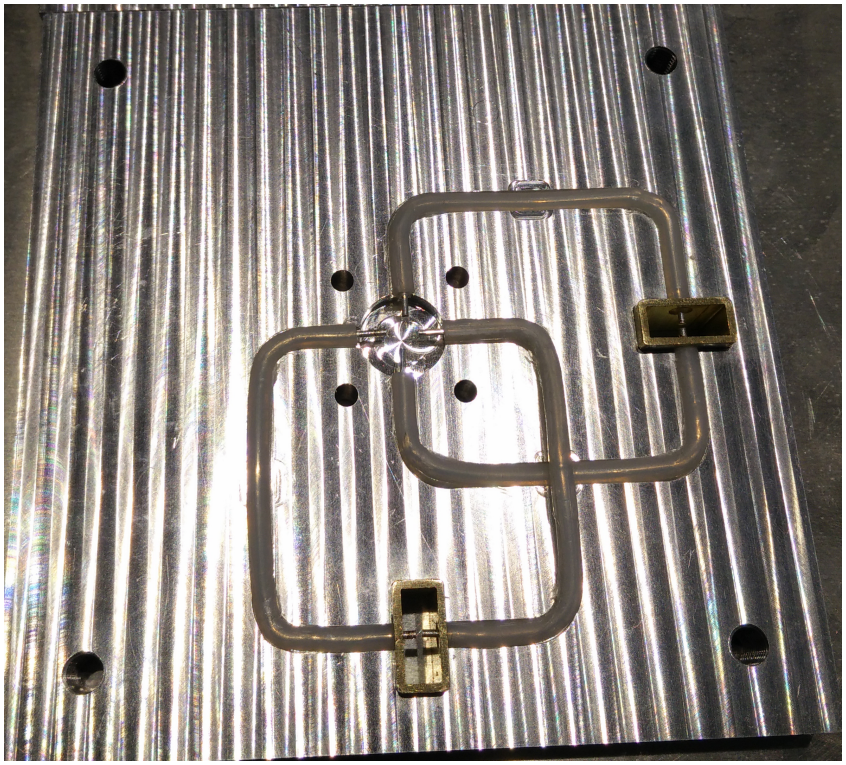

Figure 25: Back half of the OMT with waveguides and transmission lines fitted.

Bending the rigid cable was more difficult than anticipated and resulted in uneven lines, which might result in phase differences in the finished product. A heat gun was used to warm the transmission line and the aluminium block to fit the cable better into the slots. After fitting the transmission lines into the blocks, the probes inside the input and output ports were filed to proper lengths by hand. This will also add some unwanted inequality in the lengths of the transmission lines. The final lengths of the probes were close to the ones stated in [28]: 3.3 mm (0.13 inches) for the input port and 1.73 mm (0.068 inches) for the output ports.

9.2 Testing the OMT

A rectangular horn antenna was used as a source of horizontal and vertical polarization. According to the data sheet [34], the transmitting antenna has a gain of 20

dB. As stated earlier the receiving antenna has a calculated gain of around 27.9 dB.

Figure 26: Rotator with a horn antenna.

For outside testing a custom rotator was built using a old office chair, some aluminium plates and a jaw vice. The finished contraption can be seen in Figure 26. The transmitting antenna was rotated using the custom rotator and a regular spirit level and protractor were used to measure the rotation. The transmitting antenna was 10.4 m from the receiver. The signal was generated using R&S SMP03 signal generator and the input power to the transmitting antenna was 14.7 dBm. The result from the receiving antenna with the OMTs were measured with a GigaTronics power meter. The noise floor for this power meter was measured as roughly 70 dB. The measurement were done using different frequencies with 22 GHz being the priority. Results can seen in Table 1. If the rotation angle is marked as "NA", it means that the rotation angle was not measured because the receiving antenna was tilted to produce the maximum polarization difference in the outputs.

It can be seen that the cross-polarization isolation is from 23.0 to 37.3 dB on the measured frequencies where the maximum isolation is measured on the 22 GHz frequency. These result match quite well with the result from the OMT manufactured in [28], where from the design is adapted. Further testing with a network analyzer is needed to confirm these result and to analyse the phase balance of the probes in the OMT.

Table 1: OMT measurements done outside at the distance of 10.4 m.

Frequency	Rotation angle	P_V [dB]	P_H [dB]	ΔP[dB]
18GHz	0°	-58.7	-25.9	32.8
18GHz	90°	-27.6	-50.6	23.0
18GHz	NA	-61.1	-25.9	35.2
20GHz	NA	-53.4	-29.5	23.9
22GHz	0°	-43.2	-31.9	11.3
22GHz	45°	-32.9	-36.5	3.6
22GHz	90°	-31.2	-43.0	11.8
22GHz	NA	-26.1	-63.4	37.3
24GHz	NA	-57.8	-26.5	31.3
26GHz	90°	-28.1	-55.2	27.1
26GHz	NA	-52.6	-26.3	26.3

10 Amplifier card

10.1 Design and assembly of the amplifier card

The PCB for the mixer and amplifiers was design using CAD software called Eagle [35] by CadSoft. The idea was to keep the output lines and the lines between the amplifiers at equal length in order for the signal to have similar phase response on every path. Attenuation pads were placed between the amplifiers that one may adjust the total gain of the outputs and to prevent the board from oscillating. The voltage filtering was designed according to the specifications in the data sheets [27], [23] and [26]. The Amplifier board layout shown in the Figure 27 was ordered from Eurocircuit [36] with a stencil. The PCB was produced using Rogers 4350B [37].

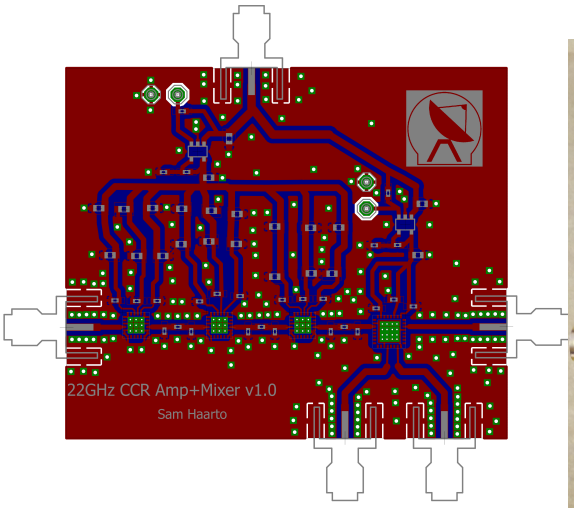

Figure 27: CAD layout of the amplifier card.

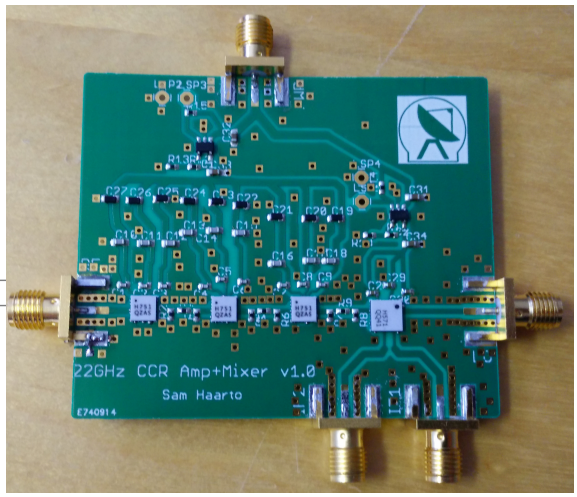

Figure 28: Assembled amplifier card.

Using the stencil was the fastest and most even way to apply the soldering paste to every solder pad on the board. The stencil was taped on top of the PCB and lined with the holes. Then soldering paste was applied on the left side of the holes and finally spread with one single motion from left to right using a razor blade. If the paste on chip pads was not sufficient or even, then the board was cleaned and the process repeated. The other soldering pads could be patched up using solder paste needle. Soldering only the chips using the stencil and then the applying the rest of the component individually was also tried but was very time consuming. Also, spreading the solder by hand resulted in a uneven layer of solder paste.

Once the components were placed onto their proper places and visually inspected, the boards were put into a re-flow oven that used the temperature curve see in Figure 29. If the paste was not even on the opposite solder pads the component could stand up or only solder to one side. Some unwanted solder balls formed from the excess solder outside the chip but this didn't seem to interfere with the workings of the microchips. The resulting PCB can be seen in Figure 28

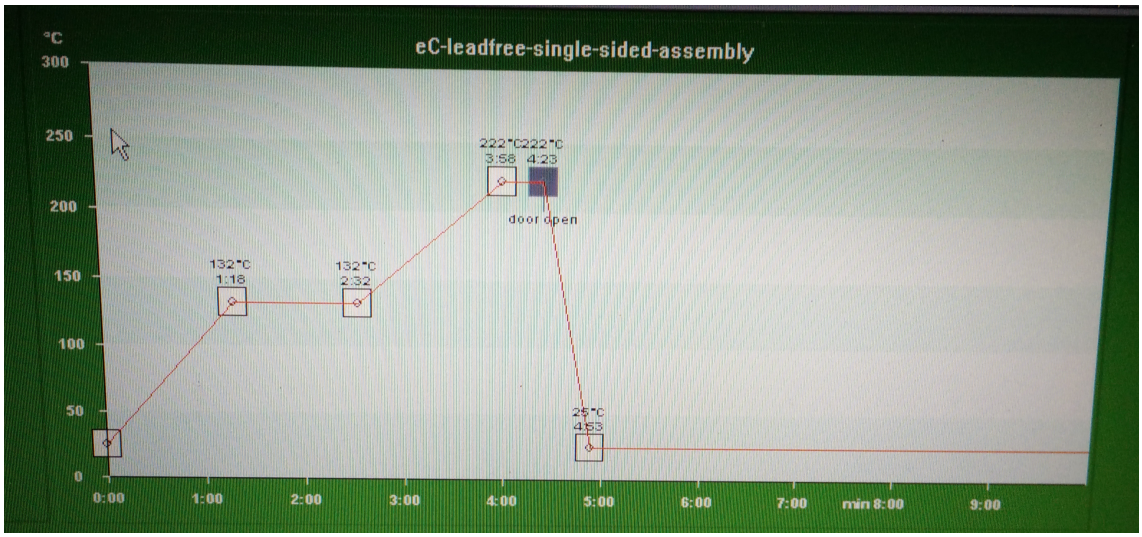

Figure 29: Temperature curve of the re-flow oven.

10.2 Testing of the amplifier PCB

The board seemed to work but the output was very low compared to the input power. Also, there was unwanted peaks on the band. Probing with an open coaxial cable it became clear that the wanted signal was only attenuating after each amplifier, however the unwanted interferences seemed to be amplified. The circuit was checked for short circuits between input and the IF output but none were found. The PCBs were annealed in the re-flow oven to make sure that everything was properly soldered but this did not improve the results.

A single amplifier from the manufactured PCB was tested by soldering off the attenuator π-pad and inserting a coaxial cable to the output line after the first amplifier. First nothing seemed to be coming out of the cable, but after pressing the cable firmly onto the board, everything seemed to be working properly. This was probably due a bad connection between the coaxial and the circuit board. After removing the losses in the cables it seemed that the amplifier was amplifying the signal but started to ring and producing harmonic signals.

One amplifier was also removed from the board to check the connections but the soldering parts seemed visually correct. When attaching the input straight to the last amplifier, everything seemed to be working with the mixer and the amplifier. However, an unwanted peak around 5 GHz was also present in the measurements. The wanted mixing result was supposed to be 500 MHz with a 21.5 GHz LO signal and a 22.0 GHz input signal. Though this 500 MHz signal could be seen in the measurement, its signal level was much lower that everything else.

10.3 Debugging the amplifier PCB

Applying Al-tape onto the transmission line seemed to stop the ringing of the amplifier card. The tape was applied on top of the input and output parts of the

transmission line to limit the resonance frequencies from forming. After much pondering the real reason for the ringing was discovered.

The 50-Ω transmission line on the amplifier card was calculated incorrectly, to be precise the line was calculated for Rogers Duroid 5880, with a dielectric constant of 2.20 [38], but the card was manufactured from Rogers 4350B with a dielectric constant of 3.66 [37]. This meant that the transmission line had an impedance of 39.96 Ω instead of the intended 50 Ω. This also explains why applying aluminium tape on the transmission line seemed to end the ringing of the amplifier card. The tape worked as a matching stub for the transmission line. This could be one way to try to fix the incorrect width of transmission lines in the amplifier cards. However, the transmission line is quite short and has little room for matching elements. Using only one element would result in a very narrow matching.

The impedance matching was improved by scraping the right amount of copper of the line to make it 0.537 mm wide, which is the correct line width for a 50-Ω line. This was done by using a scalpel and microscope. The resulting card can be seen in Figure 30. Though the width wasn't straight or even the precise width, the matching was improved and the ringing was very minimal. The down side of this operation was that the line was jagged and the adhesion between the copper line and the Polytetrafluoroethylene(PTFE) base material became weaker. The line scraping could only be done to the first part of the transmission line as there were no resistors blocking the path but this seemed to be the main contributor for the ringing.

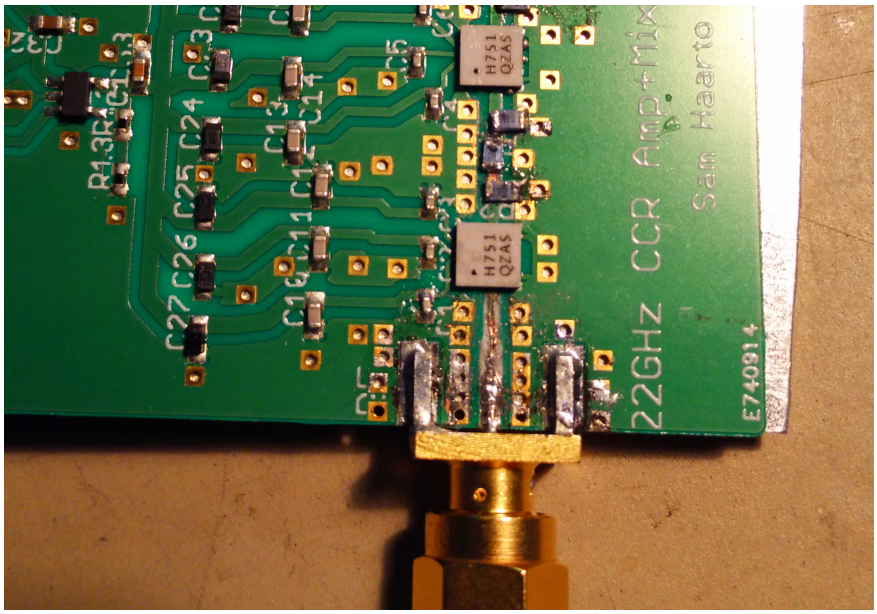

Figure 30: Amplifier PCB with the fixed line width.

The next version of the board should use the correct width for the transmission line and that should take care of the problem. However, it would be wiser to separate the three amplifiers and the mixer onto completely different boards. This would

increase the attenuation but because the amplifiers are around 25 dB it shouldn't be a problem. By separating the amplifiers onto different boards the debugging of possible new problems would become easier. Pinpointing the source of problems would be faster as the components could be tested individually where as in the current version pinpointing the source of the problems is difficult as every component is connected to each other. The amplifiers wouldn't have to be on completely separate boards but they should be able to be disconnected from the chain, either by SMA cables or some other quick-release method e.g. a switch.

If one wants to use the original design of the board one has to remember to use smaller resistors in the π-pad as the solder pad are wider than the transmission line when using the 0402 sized SMDs. One should also pay close attention to the capacitors used in the board, as their capacitance can vary large depending on the voltage used [39].

11 Conclusions and the future of the project

In this thesis, the importance of polarization in radio astronomy was explained and the astronomical purposes for polarimetry were discussed. The significance of Stokes parameters in polarization applications was shown, and the source of astronomical polarization was explained. The thesis then introduced some receiver type and then showed the process of developing a prototype receiver.

Even though the goal of producing a working prototype could not be achieved during this thesis, much can be learned from it. For future reference, one should proceed gradually and slowly when working with a limited budget. For example due to time tables and bad availability of equipment at the Department of Radio Science and Engineering (RAD) some questionable decision were made. Only one amplifier card should have been finished at a time instead of assembling them all at once just because the needed equipment happened to be available. Also, producing a testing card that houses some of the components would have been useful, instead of trying to fit all of the components to same card and hope that the end result are satisfying. As it was stated earlier, a new version of the amplifier card should be produced. It should have a modular design to ease with debugging. Also, a separate testing PCB would be beneficial.

The 180° hybrids produced were lossy but could work as long as everything else would compensate for the losses. If the produced hybrids turn out to be too lossy, one could try COTS component blocks that have the microstrip part of the hybrid. The block then needs to be fitted to a PCB with connectors. With a bigger budget the parts needed could all be bought as whole components and just assembled to make the finished prototype. Still much time should be spent reading through the data sheets and choosing connectors to ensure proper compatibility.

The OMTs were produced according to the original plan and the results seemed good. Still, due to lack of proper testing equipment the test were limited. For example the proper phase response of the OMTs still needs to be examined. The OMTs will probably need some fine tuning, to have identical phase responses on the both OMTs and on the both transmission lines of the OMTs. The fine tuning will primary consist of filing the input and output probes inside the OMTs. The antennas used in the prototype are at the moment unequal length and should be equalized.

The back-end of the receivers was supposed to be the current back-end used in VLBI but as that system has closed architecture and works unpredictably, it is clear that at least one of the ROACH2 boards needs to be ordered to proceed with the digital testing.

As for the prototype as a whole, next goal is to produce a working amplifier card and with that test the OMT and the hybrids as a system. Once a seemingly working system is produced, the digital back-end should be ordered and the phase correlation tested. When the back-end is tested properly and most of the problems have been solved, the finalizing of the designs of the continuous correlation receiver introduced in Chapter 6.6 will begin.

References

[1] Penzias, A. A. and Wilson, R. W. *A Measurement of Excess Antenna Temperature at 4080 Mc/s.* Astrophysical Journal, Volume 142, pp.419-421, July 1965. DOI:10.1086/148307

[2] Räisänen, A. V. and Lehto, A. *Radio Engineering for Wireless Communication and Sensor Applications.* ARTECH HOUSE, INC, 2003

[3] Palviainen, A. and Oja, H. *Maailmankaikkeus 2013-2014 : tähtitieteen vuosikirja. 12. vuosikerta.* Helsinki, Tähtitieteellinen yhdistys Ursa, 2012

[4] Tinberger, J. *Astronomical Polarimetry.* Cambridge University Press, 2005

[5] Lehto, A. *Radioaaltojen maailma.* Helsinki, Otatieto, 2006

[6] Wilson, T. L., Rohlfs, K., and Hüttemeister, S. *Tools of Radio Astronomy.* 6th edition. Springer, 2013

[7] *Metsähovi Radio Observatory website.* Updated: 15.1.2015, Cited: 10.1.2016, Available: http://metsahovi.aalto.fi/en/research/instruments/telescopes/

[8] Neils, S. and Le Vine, D. *Microwave Radiometer Systems : Design and Analysis.* ARTECH HOUSE INC., 2006

[9] Burke, B. F. and Graham-Smith, F. *An Introduction to Radio Astronomy.* 3rd edition. Cambridge University Press, 2009

[10] Heiles, C. *A Heuristic Introduction to Radioastronomical Polarization.* ASP Conference Proceedings. Volume 278, pp. 131-152, 2002. arXiv:astro-ph/0107327

[11] Hough, J. *Polarimetry: a powerful diagnostic tool in astronomy.* Astronomy & Geophysics, Volume 47, Issue 3, pp. 3.31–3.35, June 2006. DOI:10.1111/j.1468-4004.2006.47331.x

[12] Trippe, S. *Polarization and Polarimetry: A Review.* Journal of The Korean Astronomical Society, Volume 47, Issue 1, pp. 15-39, January 2014. DOI:10.5303/JKAS.2014.47.1.15

[13] Marscher, A. P. *Time-Variable Linear Polarization as a Probe of the Physical Conditions in the Compact Jets of Blazars.* Proceedings of IAU Symposium No. 313: "Extragalactic Jets from Every Angle," (Galapagos, Ecuador, 15-19 September 2014), pp.122-127, September 2014. DOI:10.1017/S1743921315002045

[14] Marscher, A. P., Jorstad, Svetlana G., D'Arcangelo, F. D., Smith, P. S., Williams, G. G., Larionov, V. M., Oh, H., Olmstead, A. R., Aller, M. F., Aller, H. D., McHardy, Ian M. Lähteenmäki, A., Tornikoski, M., Valtaoja, E., Hagen-Thorn, V. A., Kopatskaya, E. N., Gear, W. K., Tosti, G., Kurtanidze, O., Nikolashvili, M., Sigua, L., Miller, H. R., and Ryle, W. T. *The inner jet of an active galactic nucleus as revealed by a radio-to-γ-ray outburst.* Nature, Volume 452, pp. 966-969, April 2008. DOI:10.1038/nature06895

[15] Tiuri, M. E. *Radio Astronomy Receivers.* IEEE Transactions on Antennas and Propagation, Volume 12, Issue 7, pp. 930-938, December 1964. DOI: 10.1109/TAP.1964.1138345

[16] Räisänen, A. V. and Lehto, A. *Radiotekniikan perusteet.* 10th edition. Otatieto, 2001

[17] Mennella, A, Bersanelli, M., et.al. *Advanced pseudo-correlation radiometers for the Planck-LFI instrument.* Proceeding of 3rd ESA Workshop on millimetre wave technology and applications (ESPOO,FINLAND, 21-23 May 2003), pp.69, May 2003. arXiv:astro-ph/0307116

[18] King, O. G., Jones, M. E., Blackhurst, E. J., Copley, C. , Davis, R. J., Dickinson, C., Holler, C. M., Irfan, M. O., John, J. J., Leahy, J. P., Leech, J., Muchovej, S. J. C., Pearson, T. J., Stevenson, M. A., and Taylor, A. C. *The C-Band All-Sky Survey (C-BASS): design and implementation of the northern receiver.* Monthly Notices of the Royal Astronomical Society (MNRAS), Volume 438, Issue 3, pp. 2426-2439, March 2014. DOI:10.1093/mnras/stt2359

[19] CASPER Group *ROACH-2 Revision 2, Field-programmable gate array board.* https://casper.berkeley.edu/wiki/ROACH-2_Revision_2

[20] Wiik, K. D.Sc.(Tech). Metsähovi Radio Observatory. Metsähovintie 114, 02540 Kylmälä. Series of interviews and emails. 2015.

[21] HAT-Lab *Digital Base Band Converter.* http://www.hat-lab.com/hatlab/products/dbbc

[22] Pozar, David M. *Microwave Engineering.* 4th edition. John Wiley & Sons, Inc., 2011

[23] Hittite Microwave Corporation *HMC571LC5 - GaAs MMIC I/Q DOWNCONVERTER 21 - 25 GHz, Data sheet.* Downloaded 3.6.2015, Available: http://www.analog.com/media/en/technical-documentation/data-sheets/hmc571.pdf

[24] Analog Devices Inc. *EV-ADF5355SD1Z - Evaluation Board for Fractional-N/Integer-N PLL Frequency Synthesizer , Evaluation Board User Guide.* Downloaded 3.6.2015, Available: http://www.analog.com/media/en/technical-documentation/user-guides/EV-ADF5355SD1Z_UG-802.pdf

[25] Analog Devices Inc. *ADF5355 - Microwave Wideband Synthesizer with Integrated VCO, Data sheet.* Downloaded 3.6.2015, Available: http://www.analog.com/media/en/technical-documentation/data-sheets/ADF5355.pdf

[26] Hittite Microwave Corporation *HMC751LC4 - SMT pHEMT LOW NOISE AMPLIFIER 17 - 27 GHz, Data sheet.* Downloaded 3.6.2015, Available: http://www.analog.com/media/en/technical-documentation/data-sheets/hmc751.pdf

[27] Microchip Technology Inc. *MCP1824/MCP1824S - Low Voltage, Low Quiescent Current LDO Regulator, Data sheet.* Downloaded 30.9.2015, Available: http://ww1.microchip.com/downloads/en/DeviceDoc/22070a.pdf

[28] Engargiola, G.,Navarrini, A. *K-Band Orthomode Transducer With Waveguide Ports and Balanced Coaxial Probes.* IEEE Transactions on Microwave Theory and Techniques, Volume 53, Issue 5, pp. 1792-1801, May 2005. DOI:10.1109/TMTT.2005.847072

[29] Besser, L., Gilmore, R. *Practical RF Circuit Design for Modern Wireless Systems, Volume 1.* ARTECH HOUSE INC., 2003

[30] CST STUDIO SUITE, The electromagnetic simulation software. https://www.cst.com/Products/CSTS2

[31] Knöchel, R. and Mayer, B. *Broadband printed circuit 0° /180° couplers and high power inphase power dividers.* IEEE MTT-S International Microwave Symposium Digest, Volume 1, pp.471-474, May 1990. DOI:10.1109/MWSYM.1990.99621

[32] National Instruments *TX-LINE: Transmission Line Calculator.* http://www.awrcorp.com/products/optional-products/tx-line-transmission-line-calculator

[33] Precia Oy, Precision mechanics and CNC milling company. http://www.precia.fi/

[34] Flann Microwave *Standard Gain Horns Series 240, Data sheet.* Downloaded 10.10.2015, Available: http://www.flann.com/wp-content/uploads/2016/01/Series-240.pdf

[35] CadSoft EAGLE, PCB design software. http://www.cadsoftusa.com/

[36] Eurocircuit, PCB manufacturer. http://www.eurocircuits.com/

[37] Rogers Corp. *RO4000 Series High Frequency Circuit Materials, Data sheet.* Downloaded 19.10.2015, Available: https://www.rogerscorp.com/documents/726/acs/RO4000-LaminatesData-sheet.pdf

[38] Rogers Corp. *RT/duroid 5870 / 5880 High frequency Laminates,Data sheet.* Downloaded 19.10.2015, Available: https://www.rogerscorp.com/documents/606/acs/RT-duroid-5870-5880-Data-Sheet.pdf

[39] Fortunato, M. *Temperature and Voltage Variation of Ceramic Capacitors, or Why Your 4.7µF Capacitor Becomes a 0.33µF Capacitor.* Maxim integrated Tutorial, Updated: 4.12.2012. Cited: 19.1.2016. Available: https://www.maximintegrated.com/en/app-notes/index.mvp/id/5527